Received: 19 March 2018 | Revised: 11 August 2018 | Accepted: 20 August 2018 | Published on: 30 October 2018

DOI: 10.1002/qj.3398

RESEARCH ARTICLE

Quarterly Journal of the Royal Meteorological Society RMetS

Climatology of extreme cold events in the central Peruvian Andes during austral summer: origin, types and teleconnections

Juan Sulca[1,2] | Mathias Vuille[1] | Paul Roundy[1] | Ken Takahashi[3] | Jhan-Carlo Espinoza[2] | Yamina Silva[2] | Grace Trasmonte[2] | Ricardo Zubieta[2]

[1]Department of Atmospheric and Environmental Sciences, University at Albany-SUNY, New York, USA

[2]Subdirección de Ciencias de la Atmósfera e Hidrología, Instituto Geofísico del Perú (IGP), Lima, Peru

[3]Servicio Nacional de Meteorología e Hidrología del Perú (SENAMHI), Lima, Peru

Correspondence

Juan Sulca, Instituto Geofísico del Perú, Calle Badajoz 169, Urb. Mayorazgo IV Etapa, Ate, 15026, Peru.

Email: sulcaf5@gmail.com

The climatological and large-scale characteristics of the extreme cold events (ECEs) in the central Peruvian Andes (Mantaro basin (MB)) during austral summer (January–March) are examined using reanalysis, gridded and *in situ* surface minimum temperature (*T*min) data for the 1979–2010 period. To describe the influence of the Madden–Julian Oscillation (MJO) on ECEs in the MB, two ECE groups are defined on the basis of the sign of the outgoing long-wave radiation (OLR) anomalies in the MJO band (30–100 days, 0–9 eastward) at 12.5°S, 75°W. Type-1 ECEs occur during the suppressed convection phase of the MJO (OLR anomalies $\geq$+2 W/m^2) while Type-2 ECEs occur during the enhanced convection phase of the MJO (OLR anomalies $\leq$−2 W/m^2). ECEs in the MB are associated with the advection of cold and dry air along the east of the Andes through equatorward propagation of extratropical Rossby wave trains (ERWTs). This cold advection weakens the Bolivian High–Nordeste Low (BH-NL) system over South America (SA) at upper-tropospheric levels. The MJO is an important driver of ECEs in the MB, favouring the cold advection along the Andes during specific MJO phases. Fifty-nine per cent of Type-1 ECE's and 86% of Type-2 ECE's occur in MJO Phases 7-2. Type-1 and 2 ECEs feature a weakened BH over SA at upper-tropospheric levels. For Type-1, ERWTs emanate from southeastern Africa in MJO Phases 8-1 while ERWTs are strengthened when crossing the subtropical southern Pacific Ocean during MJO Phases 2 and 7. With respect to Type-2, MJO Phases 7-2 feature circumpolar Rossby wave trains propagating toward SA. Ultimately, MJO Phases 7-2 induce negative *T*min anomalies over MB, while MJO Phases 3-6 induce positive *T*min anomalies. El Niño and La Niña strengthen negative *T*min anomalies over the MB during MJO Phases 7-8 while they weaken positive *T*min anomalies over the MB during MJO Phases 3-6.

KEYWORDS

atmospheric teleconnections, Bolivian high, central Peruvian Andes, ENSO, extratropical Rossby waves, extreme cold episodes, MJO, southeastern Africa

1 | INTRODUCTION

The Andes are the most prominent topographic feature of South America (SA), extending from the southern tip of the continent (53°S) to northernmost Colombia (10°N). The tropical and subtropical portions of the Andes mountains have a mean maximum height around 4,000 m ASL (Garreaud *et al.*, 2009). The Andes are exposed to the tropical and extratropical upper-level large-scale circulation, characterized by moderate easterly winds at low latitudes (north of 15°S) and westerly winds at subtropical/extratropical latitudes. To the west of the central Andes, the South Pacific subtropical anticyclone produces dry and stable conditions, with moist air confined below the subsidence inversion around 900 hPa (Garreaud

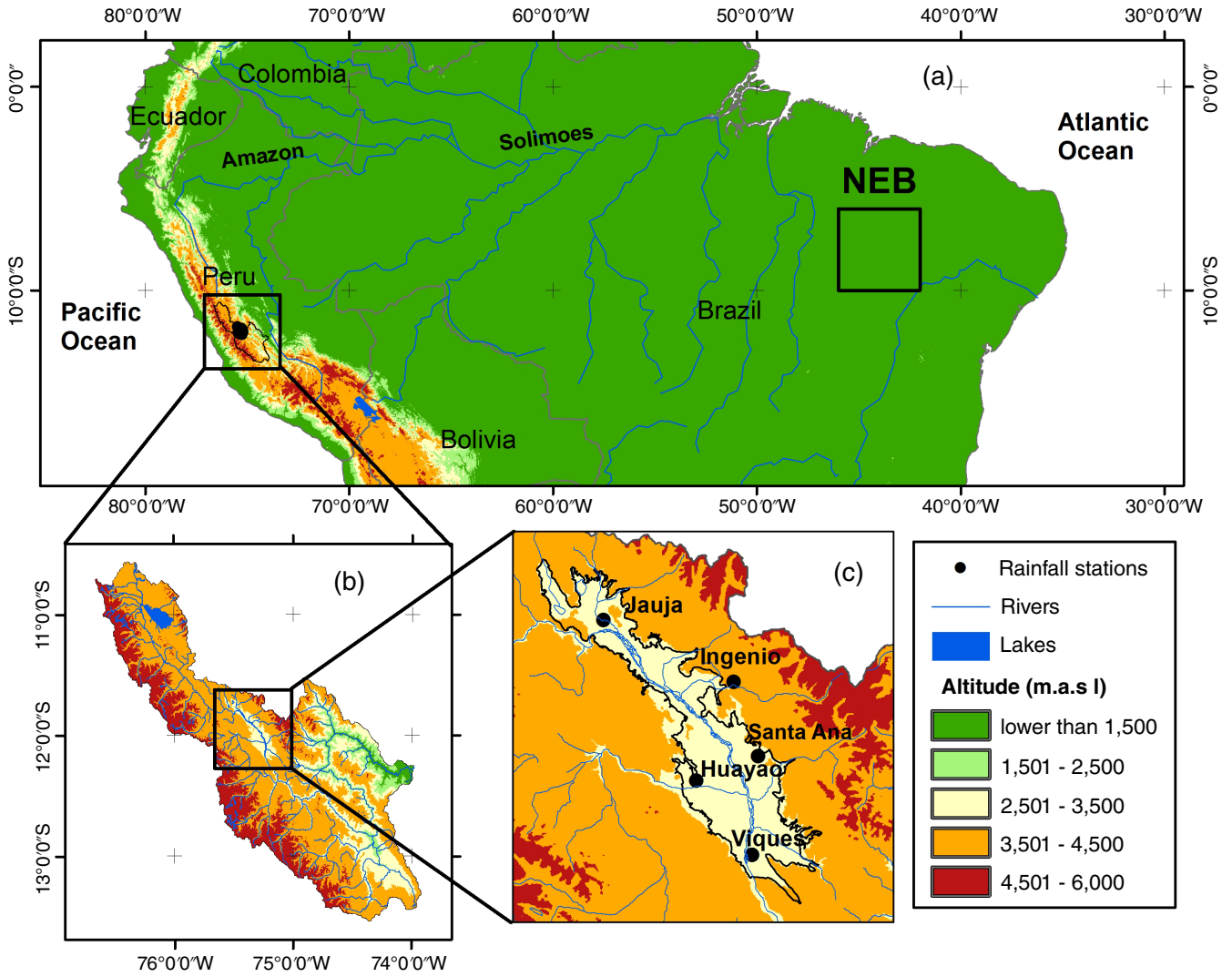

FIGURE 1 Location of Mantaro valley and all stations used in this study: (a) South America, (b) Mantaro basin, (c) and Mantaro valley. The locations of all stations used in this study are represented by black circles. Black box represents the location of northeast Brazil [Colour figure can be viewed at wileyonlinelibrary.com]

et al., 2009). The lowlands to the east of the Andes on the other hand are controlled by a heat-low with high humidity prevailing in the lower and middle troposphere (Garreaud *et al.,* 2009).

Most of the cloudiness in the central Andes appears during the austral summer (January–February–March, JFM) when mid- and upper-level easterly winds – enhanced by the strengthening of the Bolivian High – entrain near-surface upslope easterly flow. This flow is responsible for moist air influx from the Amazon basin to the central Andes, favouring increased cloudiness (e.g. Garreaud and Wallace, 1997; Garreaud *et al.,* 2003; Vuille and Keimig, 2004).

The Mantaro basin (MB) is located in the central Peruvian Andes (10°34′–13°35′S, 73°55′–76°40′W) covering an area of approximately 34,550 km^2 (Figure 1b). It is a complex Andean region with altitudes ranging from 500 to 5,350 m above sea level (ASL), and its average altitude is 3,800 m ASL. The Mantaro valley (MV) is located at 11°40′–12°10′S, 75°10′–75°15′W, covering an area of approximately 65,500 ha at 3300 m ASL (Figure 1c). MV is one of the agriculturally most productive areas of the Peruvian Andes and even entire Peru, with 77% of its entire surface area dedicated to rain-fed agriculture (Zubieta, 2010). Nonetheless, the Mantaro basin is often affected by extreme hydrometeorological events during the austral summer, such as dry and wet spells (e.g. Sulca *et al.,* 2016; Zubieta *et al.,* 2016) or floods (Zubieta *et al.,* 2012), which negatively impact local crop yields. Highest temperatures are reached during austral summer (JFM) when the average value is about 7 °C (e.g. Trasmonte *et al.,* 2010). At the same time, cloud cover over the MB also reaches a maximum. By contrast, both variables register their minimum values during austral winter (Instituto Geofísico del Peru (IGP), 2005).

During austral summer the MB frequently registers cold episodes, when the temperature drops during the night-time or early morning hours. Low temperature can damage local crops, such as happened during cold episodes in 2006, 2007 and 2011 (Giraldez and Trasmonte, 2012). In 2007 such cold episodes led to economic losses around 3 million US$ in corn and potato crops (Dirección Región Agricola - Junin,

(DRA-JUNIN), 2010). However, knowledge about the physical mechanisms associated with extreme cold events (hereafter ECEs) in the central Andes of Peru is very limited.

The Madden–Julian Oscillation (MJO) is an atmospheric, large-scale, eastward propagating circulation anomaly, originating in the western Indian Ocean, which is confined to the Tropics, moves at around 5–10 m/s and has a recurrent average duration from 30 to 90 days (Madden and Julian, 1972; 1994). The MJO registers its maximum peaks during austral summer and autumn seasons. Alvarez *et al.* (2016) have demonstrated that the MJO modulates the daily surface temperature along the Peruvian Andes during austral summer. They also documented that the MJO has two different mechanisms to lower daily surface temperature over the Peruvian Andes during austral summer. However, the results documented in Alvarez *et al.* (2016) have hitherto not been applied to investigate extreme cold episodes in the MB. Hence, here we will characterize the physical mechanisms associated with extreme cold episodes in the MB to document their dynamical link with changes in the large-scale circulation induced by the MJO. Establishing such dynamical links between local meteorological variables and the large-scale circulation might facilitate the development of a monitoring and prediction system to prevent future damage to local agriculture.

The El Niño–Southern Oscillation (ENSO) is a coupled ocean–atmosphere phenomenon originating in the tropical Pacific with global impacts. El Niño and La Niña represent the warm and cool phases of ENSO, respectively. Large-scale weather anomalies associated with El Niño and La Niña conditions have been documented around the globe through atmospheric and oceanic teleconnections, with significant impacts on society and natural systems (Ropelewski and Halpert, 1987; Trenberth *et al.,* 1998; McPhaden *et al.,* 2006).

The anomalously warm conditions in the central Pacific associated with El Niño lead to heating of the entire tropical troposphere and induce a stationary Rossby wave at upper-tropospheric levels (Gill, 1980). This Rossby wave response is characterized by a pair of anticyclones straddling the Equator with their nuclei around 140 and 130°W, respectively, easterly equatorial wind anomalies and positive equatorial geopotential height anomalies extending to the far-eastern Pacific (Garreaud and Aceituno, 2001). Recently, Sulca *et al.* (2018) showed that the stationary Rossby wave response is also observed when the warm conditions reach the far-eastern Pacific, but the stationary Rossby wave response is weaker than during warm conditions over the central Pacific. In South America Vuille *et al.* (2000) and Garreaud *et al.* (2003) pointed out that warm conditions over the central Pacific associated with El Niño increase air temperature of South America north of 20°S, which includes the Peruvian Andes. The opposite case occurs during La Niña events. However, there exist no previous studies about the influence of ENSO on extreme cold events in the Mantaro basin during austral summer. As already mentioned above for the case of the MJO, establishing a relationship between ENSO and extreme cold episodes in the MB might also contribute to the development of a seasonal prediction system, to reduce future damage to local agriculture.

Motivated by these considerations, the primary goal of this study is to assess the relationship between the large-scale circulation and extreme cold episodes in the Mantaro basin during austral summer (JFM). The second goal is to establish the relationship between ENSO and extreme cold episodes in the MB during austral summer. The third goal is to describe the impacts of the MJO on extreme cold episodes in the Mantaro Basin during austral summer. To achieve these objectives, we use *in situ* temperature data recorded at several locations in the central Peruvian Andes during the period 1979–2010.

The article is organized as follows. Section 2 contains the scientific background for our study. Section 3 discusses the data and methods that were applied. Section 4 presents the results from our composite analysis for atmospheric circulation patterns linked to extreme cold episodes during austral summer (JFM). Section 5 presents the different types of cold episodes that occur in the MB during austral summer, while Section 6 takes a closer look at the impacts of the MJO phase during different ENSO states on extreme cold episodes in the Mantaro Basin. Finally, the last section discusses the results, summarizes this study and ends with some conclusions.

2 | BACKGROUND

During the austral summer, the atmospheric circulation in South America (SA) is characterized by the development of the South American Monsoon System accompanied by enhanced convective activity, mainly over the central Amazon (e.g. Vera *et al.,* 2006; Garreaud *et al.,* 2009; Marengo *et al.,* 2012).

The upper-level atmospheric circulation over South America during the austral summer (JFM) is characterized by a large-scale system called Bolivian High–Nordeste Low (BH-NL) system (Chen *et al.,* 1999). The Bolivian High is an upper-tropospheric anticyclonic circulation caused by the latent heat released during deep convection over the Amazon basin (Lenters and Cook, 1997). The Nordeste Low is an upper-level cyclone located near the northeast coast of Brazil. This vortex over northeastern Brazil (NEB) is associated with net subsidence, compensating the intense upward vertical motion during the rainy season over the Amazon basin according to regional energy balance studies (Kousky and Gan, 1981). The BH-NL system disappears during the austral winter because of strengthened westerly zonal flow over all of South America (Garreaud *et al.,* 2009).

Another main feature is the South Atlantic Convergence Zone (SACZ). The SACZ is an elongated convective area located between 20–40°S and 50–20°W. The SACZ is observed all year, forced by synoptic-scale wave trains from midlatitudes (Liebmann *et al.,* 1999; Carvalho *et al.,* 2004; Espinoza *et al.,* 2012), but it is most active during austral

summer (e.g. Kodoma, 1992; Figueroa *et al.,* 1995; Carvalho *et al.,* 2004).

On synoptic time-scales (<5 days), the strength and shape of the BH-NL system is modulated by several phenomena such as midlatitude extratropical Rossby waves. For instance, the equatorward propagation of extratropical Rossby wave trains from midlatitudes toward the Tropics along the eastern coast of South America modulates the location, strength and shape of the BH (Garreaud, 1999a). Furthermore, these extratropical Rossby wave trains also modulate the intensity and location of the SACZ (e.g. Kousky, 1979; Liebmann *et al.,* 1999; Carvalho *et al.,* 2004) as well as the spatial distribution of the rainfall over the Amazon basin, including the Peruvian Amazonia (Espinoza *et al.,* 2012; Paccini *et al.,* 2018).

Cut-off lows are defined as closed lows that have detached from the main westerly current of air and taken a position equatorward of this current. In South America, cut-off lows have a short duration (up to 3 days) and a high likelihood of occurrence at 200 hPa (Reboita *et al.,* 2010). Cut-off lows have a marked seasonal cycle with a minimum frequency during austral summer (Fuenzalida *et al.,* 2005). Cut-off lows might induce moderate but unseasonal rainfall along the semi-arid western slope of the Andes cordillera at altitudes above 5,000 m ASL (Garreaud and Fuenzalida, 2007). However, these studies did not establish any dynamical link between cut-off lows and extreme cold episodes in the central Peruvian Andes during austral summer.

Cold surges are defined as the incursion of cold and dry air masses from the southernmost part of the continent toward low latitudes. In South America, several observational and numerical studies have documented how cold surges can lead to a dramatic drop in air temperature along their trajectory during their northward propagation (Garreaud and Wallace, 1997; Garreaud, 1999a; 1999b; 2000; Lupo *et al.,* 2001; Garreaud *et al.,* 2003; 2009; Metz *et al.,* 2013). Trasmonte *et al.* (2008) documented that the local population of the central Peruvian Andes assumes that incursions of cold and dry air masses represent the main physical mechanism to generate cold episodes in the MB during austral summer. In contrast, Montes de Oca (1995) pointed out that cold surges sometimes generate sporadic precipitation events during their propagation along the eastern slope of the Bolivian central Andes. Similarly, Hurley *et al.* (2015) documented that around 70% of the total snow accumulation on the Quelccaya ice cap, which is located in the Peruvian Andes at 5,680 m altitude, is associated with cold air incursions. Recently, Sicart *et al.* (2016) documented how low-level southerly wind incursions along the eastern side of the central Andes enhance cloud cover over the Bolivian Andes by ∼46%. These summer incursions of midlatitude air into subtropical and tropical South America provoke a significant enhancement of cloud cover along the eastern slope of the Andes, as well as a northeastward displacement of the SACZ (Garreaud and Wallace, 1997) during their northward propagation.

Several studies have documented how sea-surface temperature (SST) anomalies over the South Indian and Pacific Oceans affect precipitation over South America during austral summer through propagation of extratropical Rossby wave trains (Berbery *et al.,* 1992; Hoskins and Ambrizzi, 1993; Ambrizzi and Hoskins, 1997; Drumond and Ambrizzi, 2008). For example, Drumond and Ambrizzi (2008) identified how SST anomalies in three regions located in the Indian Ocean (southeastern Africa), the southern Pacific and the equatorial Pacific (western Pacific Ocean and southwestern South Pacific) affect precipitation over SA during austral summer. The first region is located off the coast of southeastern Africa. Warm waters over this region induce wet conditions over subtropical SA. The extratropical Rossby wave train emanates from the Indian Ocean toward SA. The second region is Indonesia. Warm SST anomalies over this region induce drought conditions over the SACZ while at the same time promoting wet conditions over the South American subtropics, through propagation of a Pacific–South America-like (PSA) wave pattern, emanating from the western Pacific. The third region is located over the southwestern South Pacific. Warm water over this region favours wet conditions over the SACZ and drought conditions over subtropical SA. Again, a PSA-like wave train emanates from Indonesia and propagates toward SA. However, the above-mentioned studies did not assess the impact of changing SST over these three regions on daily minimum temperature over the central Peruvian Andes during austral summer.

Approaches to monitor and predict the MJO increasingly rely on standardized metrics to define its spatio-temporal behaviour. One such approach is the Real-time Multivariate MJO index created by Wheeler and Hendon (2004; hereafter WH2004). This index consists of a pair (RMM1, RMM2) of empirical orthogonal functions (EOFs), which are calculated from the combined fields of near-equatorially averaged 850 hPa zonal wind, 200 hPa zonal wind, and outgoing long-wave radiation (OLR) data. This MJO index starts in 1974 because of the lack of OLR data prior to that date (Gruber and Krueger, 1984). This dataset is freely available at http://www.bom.gov.au/climate/mjo/graphics/rmm.74toRealtime.txt.

WH2004 show that RRM Phase-1 features the convection of a decaying MJO event in the central Pacific while enhanced convection of a growing event is observed over Africa and the western Indian Ocean. During the subsequent RMM Phases, the convection over the Indian Ocean develops and moves to the east, and, as it passes by the Australian land mass, shifts southward to be most concentrated around 15°S (RMM Phase 5). Eastward movement of the 850 hPa wind anomalies is quicker. Thus, enhanced convection in RMM Phases 2 and 3 (over the Indian Ocean) is in near quadrature with the wind, while in RMM Phase 7 it is wholly encompassed within the westerlies (over the Pacific). In contrast, RMM Phases 1 and 2 feature enhanced convection over the western Indian Ocean, thereby contributing to the formation of midlatitude Rossby wave trains that propagate toward the southernmost

part of the South American continent (Roundy, 2012b; see Figure 14.1).

In South America, few studies exist regarding the impacts of the MJO on daily surface temperature during austral summer. For instance, Alvarez *et al.* (2016) show that the MJO may lead to a drop in daily surface temperature along the Peruvian Andes from RMM Phase 8 to 3 during austral summer. These RMM Phases are characterized by quite different regional circulation patterns over SA thus leading to two different mechanisms associated with ECEs over Peru. The first mechanism represents an enhancement of large-scale subsidence over the Peruvian Andes as a consequence of enhanced convective activity over tropical South America, resulting from an eastward propagation of the MJO from the western Pacific Ocean toward tropical South America (e.g. from RRM Phase 6 to 1) (see their figure 7). The second mechanism features the equatorward propagation of Rossby waves along the Andes mountains, which leads to a drop in daily surface temperature over the Andes from RMM Phase 2 to 5 (see their figure 7). The two mechanisms, however, have quite different circulation patterns at upper-tropospheric levels. For instance, the first mechanism, which results in enhanced large-scale subsidence over the Peruvian Andes, is characterized by a core of negative geopotential height centred off the coast of northern Chile at 28°S, 78°W at upper-tropospheric levels (250 hPa) (RMM Phase 8 in their figure 1). The second mechanism, on the other hand, features a wide region of negative geopotential height over western South America, emanating from Australia before being refracted equatorward and crossing the Andes and the western Amazon basin toward the Northern Hemisphere around 5°N (RMM Phase 2 in their Figure 1).

The relationship between ENSO and the MJO has been extensively studied (Kessler, 2001; Moon *et al.,* 2011; and others). During the mature phase of El Niño events, the MJO activity shifts eastward into the central Pacific, and thus there is an expansion of the longitudinal domain of the MJO-related convective activity (Kessler, 2001; Moon *et al.,* 2011). Moon *et al.* (2011) pointed out that El Niño favours the eastern propagation of the MJO from RMM Phase 5 to 8 while it inhibits MJO propagation from RMM Phases 1 to 4 due to El Niño-induced enhancement of meridional baroclinicity, which weakens the upper-level easterly flow over equatorial and tropical SA. Conversely, La Niña episodes lead to enhanced upper-level easterly flow over equatorial and tropical SA and thus inhibit MJO events over equatorial and tropical SA from Phases 5 to 8. The opposite is observed from Phase 1 to 4 during La Niña.

Few studies exist about the combined impacts of concurrent ENSO events and MJO phases on minimum temperature anomalies over SA during austral summer. For example, Shimizu and Ambrizzi (2016) pointed out that El Niño weakens the negative minimum temperature anomalies over the central and southern Peruvian Andes during RMM Phase 1. Conversely, La Niña strengthens the negative minimum temperature anomalies present over the central Peruvian Andes in RMM Phase 1. La Niña also induces negative minimum temperature anomalies over all of the Peruvian Andes and Bolivian Altiplano in RMM Phase 3. The lack of statistically significant minimum temperature anomalies over the central Peruvian Andes during the other RMM Phases concurrent with El Niño and La Niña events is attributed to the inadequate resolution of reanalysis data over the complex topography of the Andes Mountains.

TABLE 1 List of meteorological stations used in this study

Station	Latitude (°S)	Longitude (°W)	Altitude (m.a.s.l.)	Period	Source
Huayao	12.04	75.32	3,308	1979–2010	IGP
Jauja	11.78	75.47	3,322	1993–2010	SENAMHI
Santa Ana	12.00	75.47	3,295	1993–2010	SENAMHI
Ingenio	11.88	75.26	3,450	2001–2010	SENAMHI
Viques	12.16	75.23	3,186	2001–2010	SENAMHI

Note. IGP: Peruvian Geophysical Institute – Peru; SENAMHI: National Service of Meteorology and Hydrology – Peru.

3 | DATA AND METHODOLOGY

We used daily minimum temperature and NCEP/NCAR daily reanalysis data to describe the extreme cold episodes in the central Peruvian Andes.

Observational daily minimum temperature (hereafter *T*min) data were obtained from five stations located within the Mantaro valley. The data were obtained from the Peruvian National Meteorology and Hydrology Service (SENAMHI) and the Peruvian Geophysical Institute (IGP) (Figure 1). Station names and length of each record are listed in Table 1. All data were previously quality-controlled at these institutions. The selected station records contain less than 5% missing values in their JFM time series.

To describe the large-scale circulation associated with extreme cold episodes in the central Peruvian Andes during austral summer, we used daily National Centers for Environmental Prediction/National Center for Atmospheric Research (NCEP-NCAR) reanalysis data (Kalnay *et al.,* 1996) of minimum surface temperature, geopotential height, and zonal and meridional wind at surface and 200 hPa levels. Data were extracted from the original dataset at 1200 UTC for the period 1979–2010. The 1200 UTC observation time was chosen because cold episodes occur between the night-time and early morning (Trasmonte *et al.,* 2008; Saavedra and Takahashi, 2017). To study the changes in cloud cover during cold episodes in the MB, we used daily OLR data from NCAR/National Oceanic and Atmospheric Administration (NOAA) (Liebmann and Smith, 1996) for the period 1979–2010. To study the equatorward propagation of cold air masses to the east of the Andes mountains during extreme cold episodes in the MB, we computed total temperature advection for the same period.

We defined extreme cold events in the central Peruvian Andes during austral summer as periods when the *T*min of Huayao ≤2.5 percentile of the daily summer temperature distribution (about 2.5°C). The selection of Huayao station was motivated by the fact that its minimum temperature shows a strong linear correlation ($r \geq 0.77$, $p < 0.05$) with the rest of the stations located within the Mantaro basin during JFM for the period 2001–2010. Finally, we replaced missing data in the Huayao station record with the value of the linear regression of minimum temperature between Huayao and Santa Ana station, given its nearby location. We used this criterion as it had been applied successfully in a previous study regarding the incursion of cold surges in the Peruvian Amazon during austral winter (Espinoza *et al.,* 2013). The number of data replaced is <0.2% over the entire period. For Peru, we used PISCO (Peruvian-interpolated data of the SENAMHI's climatological and hydrological observations: Huerta *et al.,* 2017) daily gridded minimum temperature dataset, which has a horizontal resolution of $0.05° \times 0.05°$ for the period 1981–2016 and is based on the Tmin-gauge network data of the Servicio Nacional de Meteorología e Hidrología (SENAMHI) (freely available at ftp://ftp.senamhi.gob.pe/PISCO_temperatura).

A forecast system for tracking and prediction of large-scale organized tropical convection such as the MJO can be obtained by a two-step space–time EOF technique (Roundy, 2012a). Roundy (2012a) defined as enhanced (suppressed) convection periods in the MJO band (30–100 days, wave numbers 0–9 eastward) when negative (positive) OLR anomalies are equal to or lower than -2 W/m^2 ($\geq +2$ W/m^2). Thus, we classified ECEs in the MB into two groups: Type-1 episodes occur during periods of enhanced convection in the MJO band, while Type-2 episodes occur during periods of suppressed convection. Only extreme cold episodes, which coincide with active MJO ($\sqrt[2]{RMM1^2 + RMM2^2} \geq 1$: WH2004), were analysed.

To characterize the change of SST over the Southern Hemisphere during ECEs in the Mantaro basin, we used daily anomalies of SST from NOAA (Reynolds *et al.,* 2007). This dataset has a horizontal resolution of $0.25° \times 0.25°$ and is available starting in 1981. It can be downloaded freely at https://www.esrl.noaa.gov/psd/data/gridded/data.noaa.oisst.v2.highres.html.

To establish potential relationships between extreme cold episodes in the Mantaro basin and ENSO during austral summer, we used the Niño 3.4 index from the Climate Prediction Center (CPC) (Smith *et al.,* 2008) for the same period 1979–2010.

ENSO conditions were defined according to the Oceanic Niño Index provided by NOAA. Thus, each year was categorized as Neutral, El Niño, or La Niña (http://origin.cpc.ncep.noaa.gov/products/analysis_monitoring/ensostuff/ONI_v5.php).

To identify the source of the extratropical Rossby wave trains associated with Type-1 and 2 ECEs in the Mantaro basin during the austral summer, we used the diagnostic tool called wave-activity flux (Plumb, 1985) that is based in quasi-stationary Rossby wave propagation theory. Following the Schubert and Park (1991) definition, the horizontal flux components that are applicable for quasi-geostrophic stationary waves on a zonal flow are:

$$F_\lambda = \frac{p}{2000a^2 \cos\varphi}\left[\left(\frac{\partial\psi'}{\partial\lambda}\right)'^2 - \psi'\frac{\partial^2\psi'}{\partial\lambda^2}\right], \quad (1a)$$

$$F_\varphi = \frac{p}{2000a^2}\left(\frac{\partial\psi'}{\partial\lambda}\frac{\partial\psi'}{\partial\varphi} - \psi'\frac{\partial^2\psi'}{\partial\lambda\partial\varphi}\right), \quad (1b)$$

where p is pressure, φ is latitude, λ is longitude, a is the radius of the Earth, ψ is the stream function, and primes denote deviation from the zonal mean (the "eddy" component). Wave activity fluxes are parallel to the group velocity and their convergence indicates the piling up of the wave activity, while fluxes' divergence indicates its export (Plumb, 1985). This approach has been extensively used in both model and observational studies (Takaya and Nakamura, 2001; Vera *et al.,* 2004; Junquas *et al.,* 2016).

Ultimately, compositing techniques and Superposed Epoch Analysis were applied to identify anomalous large-scale atmospheric circulation, cloud cover, and minimum temperature associated with these cold episodes and to characterize the mechanisms responsible for producing them in the central Peruvian Andes. We applied a Student's *t*-test (Wilks, 2011) to verify the statistical significance of the results.

4 | CLIMATOLOGICAL FEATURES OF EXTREME COLD EPISODES IN THE MB

We identified 56 extreme cold episodes in the central Peruvian Andes with an average duration of 1.49 days.

Figure 2 shows the results from a Superposed Epoch Analysis of *T*min during extreme cold episodes (ECEs) in the MB during austral summer for the period 1979–2010. Figure 2a illustrates that extreme cold episodes in the MB are short-lived, with *T*min dropping sharply to 1.97 ± 0.86°C below average from day −1 to day 0 (considering day 0 as the day where *T*min ≤ 2.5°C) but recovering quickly from day 0 to day +1. Figure 2a also illustrates that temperature recovery is observed at day +2 and +3, but at day +3 the temperature anomaly is no longer statistically significant. Figure 2b shows the histogram associated with the duration of ECEs in the MB (in per cent). It illustrates the short-lived nature of ECEs in the MB, with 91.08% of all ECEs lasting less than two consecutive days. By contrast, only 1.78% of all cold episodes show a duration of five or more consecutive days. Hence, an ECE in the Mantaro basin tends to be a very short-lived phenomenon.

Figure 3 illustrates the results of the composite analysis, highlighting the large-scale atmospheric circulation associated with ECEs in the MB. Figure 3a shows the predominance of negative *T*min anomalies over the tropical Andes (northern

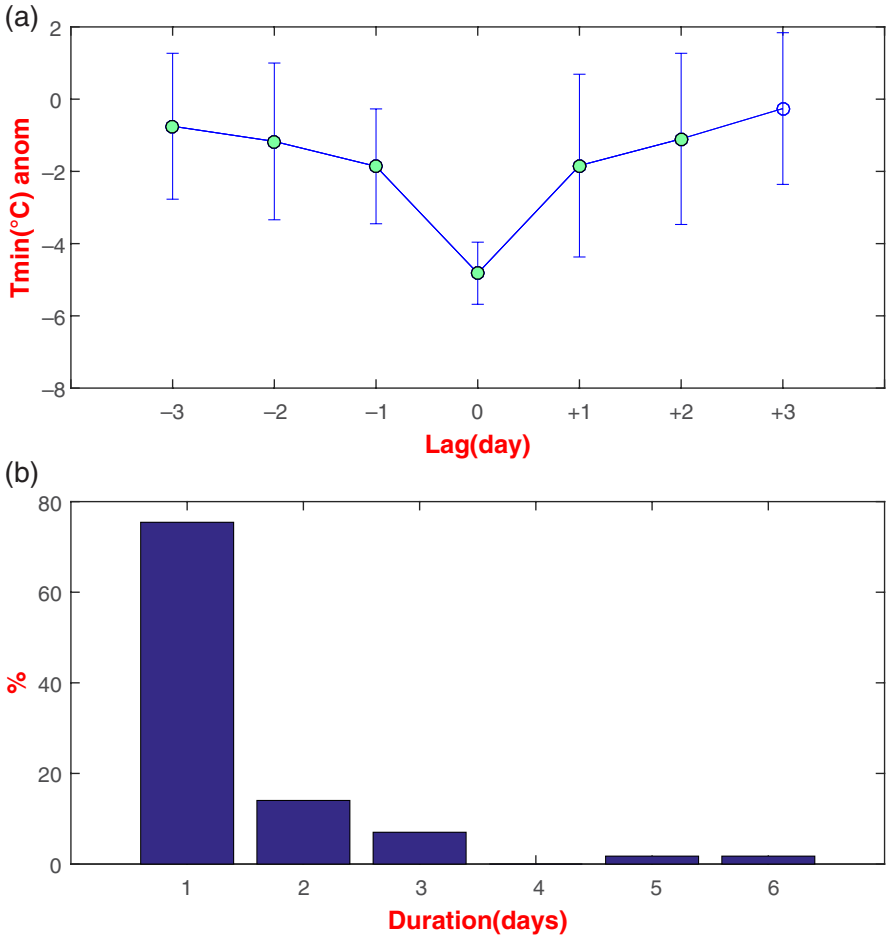

FIGURE 2 (a) Superposed epoch analysis applied to daily minimum temperature anomalies for extreme cold episodes in the central Peruvian Andes during austral summer (January–February–March). (b) Histogram of the duration of extreme cold episodes in the central Peruvian Andes during the austral summer. Green circles represent days where minimum temperature anomalies are statistically significantly different from zero at 95% confidence level based on Student's *t*-test. Data of minimum temperature of Huayao station was used in this study. Analysis based on the period 1979–2010 [Colour figure can be viewed at wileyonlinelibrary.com]

Bolivian Andes, Peruvian Andes, and Ecuadorian Andes) during ECEs in the MB. Figure 3b documents negative *T*min anomalies over the southern and central Peruvian Andes, which even extend toward southeastern Brazil and the South Atlantic. Figure 3b also illustrates positive *T*min anomalies over parts of northeastern Brazil (NEB). This *T*min pattern is consistent with positive OLR anomalies over the Peruvian Andes, which extend toward the southern Colombian Andes and off the coasts of Peru and northernmost Chile toward 100°W; while OLR anomalies of the opposite sign prevail over NEB and the western tropical Atlantic (Figure 3d). The negative *T*min anomalies over the central Peruvian Andes in the PISCO and reanalysis datasets are consistent with station-based findings of cold conditions over the study area, but also show that negative temperature anomalies extend over a larger part of the central Peruvian Andes than just the Mantaro basin itself. The negative *T*min anomalies present along the Andes Mountains are consistent with the negative temperature advection and southeasterly surface wind anomalies while at the same time positive temperature advection and northwesterly wind anomalies are observed over NEB at the surface (Figure 3c). This pattern suggests that ECEs in the MB are caused by the northward advection of cold and dry air from the southernmost part of the continent along the Andes Mountains, while at the same time enhancing convective activity and cloud cover over central NEB, potentially tied to a northward displacement of the SACZ.

The cold advection inhibits cloud formation and convective activity in the study area as well as the intrusion of humidity from the Amazon basin and thus leads to a large temperature drop at night-time or early morning. At the same time, warm advection is observed over the southeastern coast of NEB, suggesting enhanced convective activity and cloud cover over this region, linked to a northeastward displacement of the climatological position of the SACZ (Carvalho *et al.,* 2004). The *T*min dipole between the MB and NEB agrees with an OLR dipole of positive OLR anomalies located over the study area while negative OLR anomalies persist over NEB (Figure 3d).

These surface circulation anomalies agree with the weakening of the mid- tropospheric zonal flow over the study area due to the predominance of 200 hPa westerly wind anomalies that extend across South America toward the tropical Atlantic (Figure 3d). Figure 3d shows that 200 hPa westerly wind

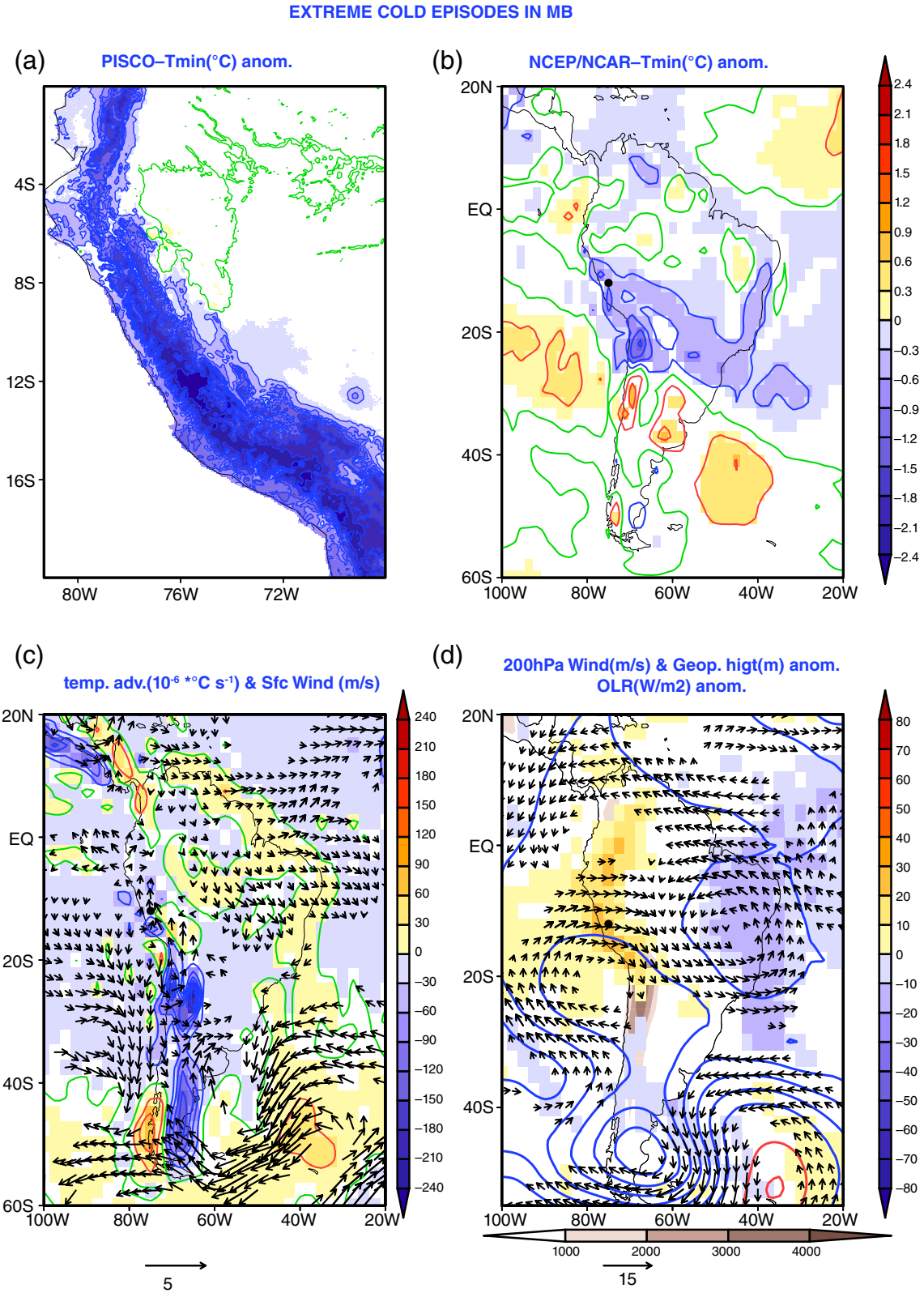

FIGURE 3 Composite anomalies during extreme cold episodes in the MB for minimum surface temperature (°C) anomalies using (a) PISCO dataset and (b) NCEP-NCAR reanalysis, (c) surface temperature advection (10^{-6}*°Cs^{-1}) and surface wind (m/s) anomalies, and (d) OLR (W/m^2) and 200 hPa wind (m/s) and geopotential height anomalies (blue (red) contours for negative (positive) anomalies, contour interval is 10 gpm, 0-contour omitted). Only minimum surface temperature, temperature advection, OLR, and wind anomalies statistically significant at the 90% confidence level are shown. Confidence-level based on a two-sided Student's *t*-test. Black dot represents the location of Mantaro Basin. Analysis based on NCEP-NCAR reanalysis dataset during the austral summer (January– March) for the 1979–2010 period. PISCO dataset was used in this study for the 1981–2010 period [Colour figure can be viewed at wileyonlinelibrary.com]

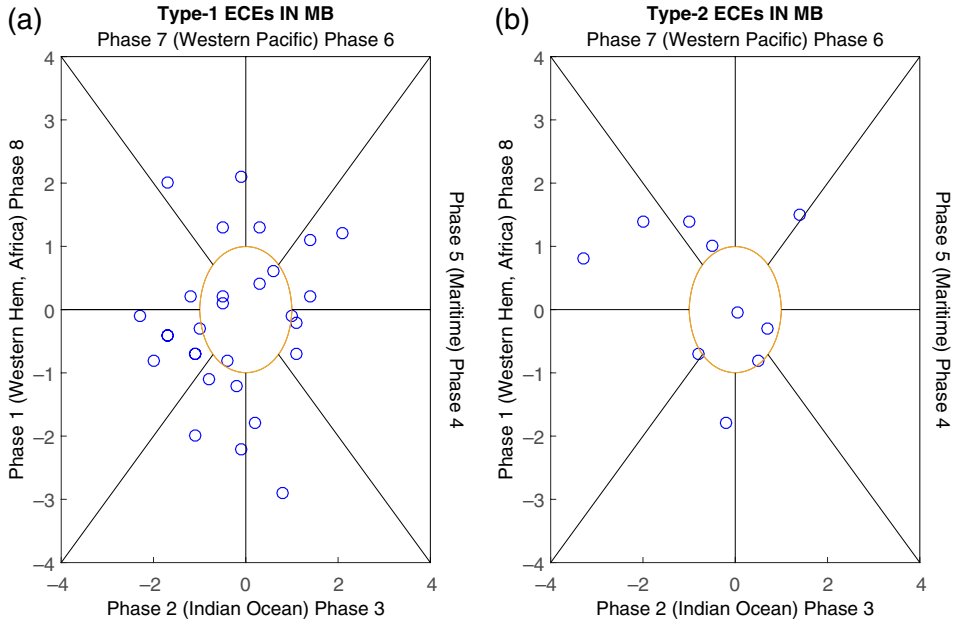

FIGURE 4 (RMM1, RMM2) phase space points for all (a) Type-1 and (b) Type-2 extreme cold episodes in the Mantaro basin. Eight defined regions of the phase space are labelled. ECEs in the Mantaro basin that are associated with a weak MJO are located inside the yellow circle. Analysis based on 1979–2010 period [Colour figure can be viewed at wileyonlinelibrary.com]

anomalies observed over the study area and the southern Peruvian Andes are associated with a cyclonic circulation centred off the coasts of southern Peru and northern Chile (22°S, 85°W). This latter signal suggests the presence of cut-off lows during the ECEs in the MB. Figure 3d also shows an anomalous anticyclonic circulation east of the Nordeste Low. These circulation anomalies are consistent with the weakening of the Bolivian High–Nordeste Low system at upper-tropospheric levels (Chen *et al.,* 1999) during the days of occurrence of extreme cold episodes in the MB. These results show that extreme cold episodes in the MB are caused mainly by anomalous incursions of cold and dry air masses, advected from the southernmost part of South America (Garreaud, 1999b; 2000; Trasmonte *et al.,* 2008; Metz *et al.,* 2013), while few extreme cold events in the MB are caused by cut-off lows (Fuenzalida *et al.,* 2005; Garreaud and Fuenzalida, 2007) or dry spell events in the MB (Sulca *et al.,* 2016). The specific regional processes associated with cut-off lows and dry spells in the MB for the generation of ECEs in the MB during austral summer will not be considered in the remainder of the analysis.

5 | TYPES OF EXTREME COLD EPISODES OVER THE MB DURING AUSTRAL SUMMER

5.1 | Statistical features

The results of a statistical analysis of the number of ECEs in the MB associated with suppressed and convective events in the MJO band show that 69.39% of all ECEs in the MB are associated with suppressed or enhanced convective events in the MJO band, with Type-1 (suppressed convective episodes) representing 48.98% of all ECEs in the MB, and Type-2 (enhanced convective episodes) representing 20.41% (figure not shown). Hence, the MJO tends to be correlated with ECEs in the central Peruvian Andes during austral summer.

The results of the identification of MJO Phases during the initial day (day-0) of each Type-1 and 2 extreme cold episodes in the MB are shown in Figure 4. Figure 4a documents that 81.5% of Type-1 ECE's and 70% of Type-2 ECE's coincide with an active MJO (Figure 4b). The remaining percentage of Type-1 (18.5%) and Type-2 ECEs (30%) in the MB will not be considered in the remainder of the analysis.

The results of a statistical analysis of the number of Type-1 and Type-2 extreme cold episodes in the MB during each MJO Phase in austral summer (in per cent) are shown in Figure 5. Figure 5a illustrates that RMM Phase 1 represents 23% of all Type-1 episodes, RMM Phase 2 represents 18.2%, RMM Phase 3 represents 9%, RMM Phases 4, 5 and 7 each represent 13.6%, and RMM Phases 6 and 8 both represent 4.5%. With respect to Type-2 ECE's, Figure 5b shows that RMM Phases 1, 2 and 6 each represent 14.3% of Type-2 ECE's, RMM Phases 3, 4 and 5 each represent 0%, and RMM Phases 7 and 8 both represent 28.5%. These results suggest that Type-2 ECE's are favoured by RMM Phases 6-8 and 1-2, while Type-1 ECE's in the MB during austral summer are more randomly distributed across RMM phases.

5.2 | Large-scale atmospheric circulation features

A composite analysis for anomalous fields of surface *T*min, surface wind, temperature advection, OLR, and geopotential height and wind at 200 hPa was performed to identify the role of the episodes with enhanced and suppressed convection in the MJO band in producing Type-1 and -2 extreme cold

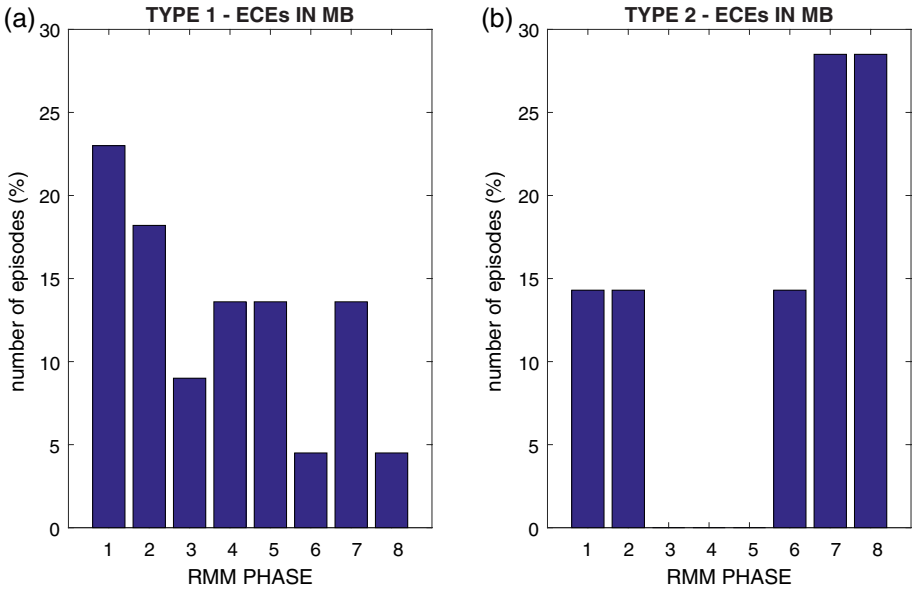

FIGURE 5 Histogram of the number of ECEs in the MB during each RMM Phase for (a) Type-1 ECEs and (b) Type-2 ECEs. Analysis based on Type-1 and -2 ECEs that occur during active MJO phases only (e.g. $\sqrt[2]{RMM1^2 + RMM2^2} \geq 1$). Analysis based on 1979–2010 period [Colour figure can be viewed at wileyonlinelibrary.com]

episodes in the MB (Figures 6 and 7, respectively). Figure 6a shows that Type-1 extreme cold episodes in the MB are characterized by negative *T*min anomalies stretching from the Ecuadorian Andes to northern Chile, while at the same time a sequence of negative and positive *T*min anomalies is apparent along the east coast of SA, stretching from the southern tip toward NEB (Figure 6b). During Type-2 episodes (Figure 7a), negative *T*min anomalies also are observed, again affecting the entire central Andes region from the Ecuadorian Andes to northern Chile in the PISCO dataset.

Furthermore, Figure 6b also shows that Type-1 ECE's feature an elongated band of negative *T*min anomalies in the northwest–southeast direction extending from southeastern Brazil toward the South Atlantic, indicative of an enhancement and northeastward displacement of the SACZ during the occurrence of ECEs in the MB, associated with the MJO (Carvalho *et al.,* 2004). Conversely, Type-2 episodes only present negative *T*min anomalies over the continent southward of 12°S, while positive *T*min anomalies prevail over equatorial SA northward of 10°S (Figure 7b).

Type-1 ECEs in Figure 6c feature negative temperature advection and southeasterly wind anomalies along the Peruvian Andes while positive temperature advection and northwesterly wind anomalies prevail over NEB, extending out over the equatorial Atlantic. These anomalous patterns are consistent with cold air advection over the central Peruvian Andes, which extends toward the southern Colombian Andes, while at the same time warm air advection is observed along the coast of NEB, originating over the South Atlantic. These results indicate that suppressed convection periods in the MJO band are linked to the northward propagation of cold and dry air masses along the Andes. During Type-2 episodes, Figure 7c negative temperature advection and southeasterly wind anomalies are apparent along the Andes Mountains while positive temperature advection and westerly surface wind anomalies dominate over NEB. These anomalous fields agree with cold air advection over the central Peruvian Andes originating over southern SA, while warm air advection is observed over NEB.

Type-1 episodes are further characterized by a weakening of the zonal flow over the study area at upper-tropospheric levels. Figure 6d shows that Type-1 events coincide with westerly wind anomalies over all of the Peruvian Andes at 200 hPa. This anomalous wind pattern is consistent with the negative geopotential height anomalies seen over the Altiplano and northern Chile. Figure 6d also shows that there is no clear anomalous anticyclonic circulation around the Nordeste Low as was observed in the composite of all ECEs in the Mantaro basin (Figure 6d). Overall these upper-air circulation anomalies indicate the predominance of a weakened Bolivian High at upper-tropospheric levels during Type-1 ECEs in the MB. During Type-2 episodes, 200 hPa westerly wind anomalies dominate over the central Peruvian Andes, but they are less well developed and appear to be associated with negative geopotential height anomalies located off the coast of southern Peru and northern Chile (Figure 7d). Figure 7d also illustrates anticyclonic wind anomalies at 200 hPa over northeastern Brazil. These circulation anomalies indicate a weakening of the BH-NL system over SA at upper-tropospheric levels during Type-2 ECEs in the MB.

Finally, we performed a superposed epoch analysis of anomalous OLR, and 200 hPa wind and geopotential height, to analyse the role of the eastward propagation of the MJO in producing Type-1 and -2 ECEs in the MB during austral summer (Figure 8). Figure 8a,c,e show OLR and 200 hPa wind and geopotential height anomalies prior to, during and following Type-1 ECEs in the MB (days −5, 0

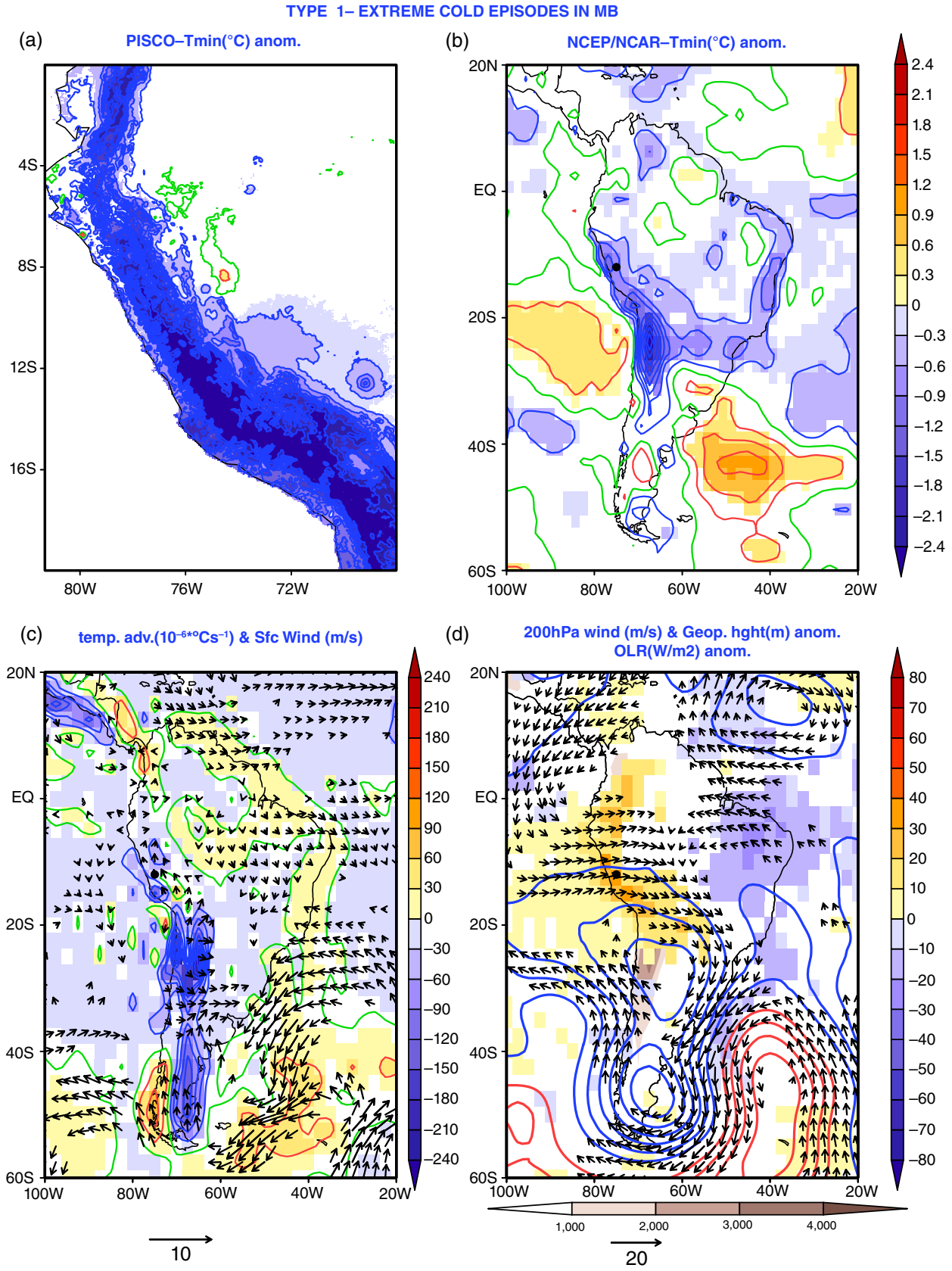

FIGURE 6 Composite anomalies during Type-1 extreme cold episodes in the MB for minimum surface temperature anomalies (°C) using (a) the PISCO dataset and (b) NCEP-NCAR reanalysis, (c) surface temperature advection (10^{-6}*°Cs^{-1}) and surface wind anomalies (m/s), and (d) OLR (W/m^2) and 200 hPa wind (m/s) and geopotential height (blue (red) contours for negative (positive) anomalies, contour interval is 10 gpm, 0-contour omitted) anomalies. Only anomalies of surface minimum temperature, temperature advection, OLR and wind that are statistically significant at the 90% confidence level are shown. Confidence-level based on a two-sided Student's *t*-test. In (d), elevations above 1,000, 2,000 and 3,000 m are indicated by light to dark brown shading. Black dot indicates location of Mantaro Basin. Analysis based on NCEP-NCAR reanalysis during austral summer (January– March) for the 1979–2010 period. PISCO dataset was used in this study for the 1981–2010 period [Colour figure can be viewed at wileyonlinelibrary.com]

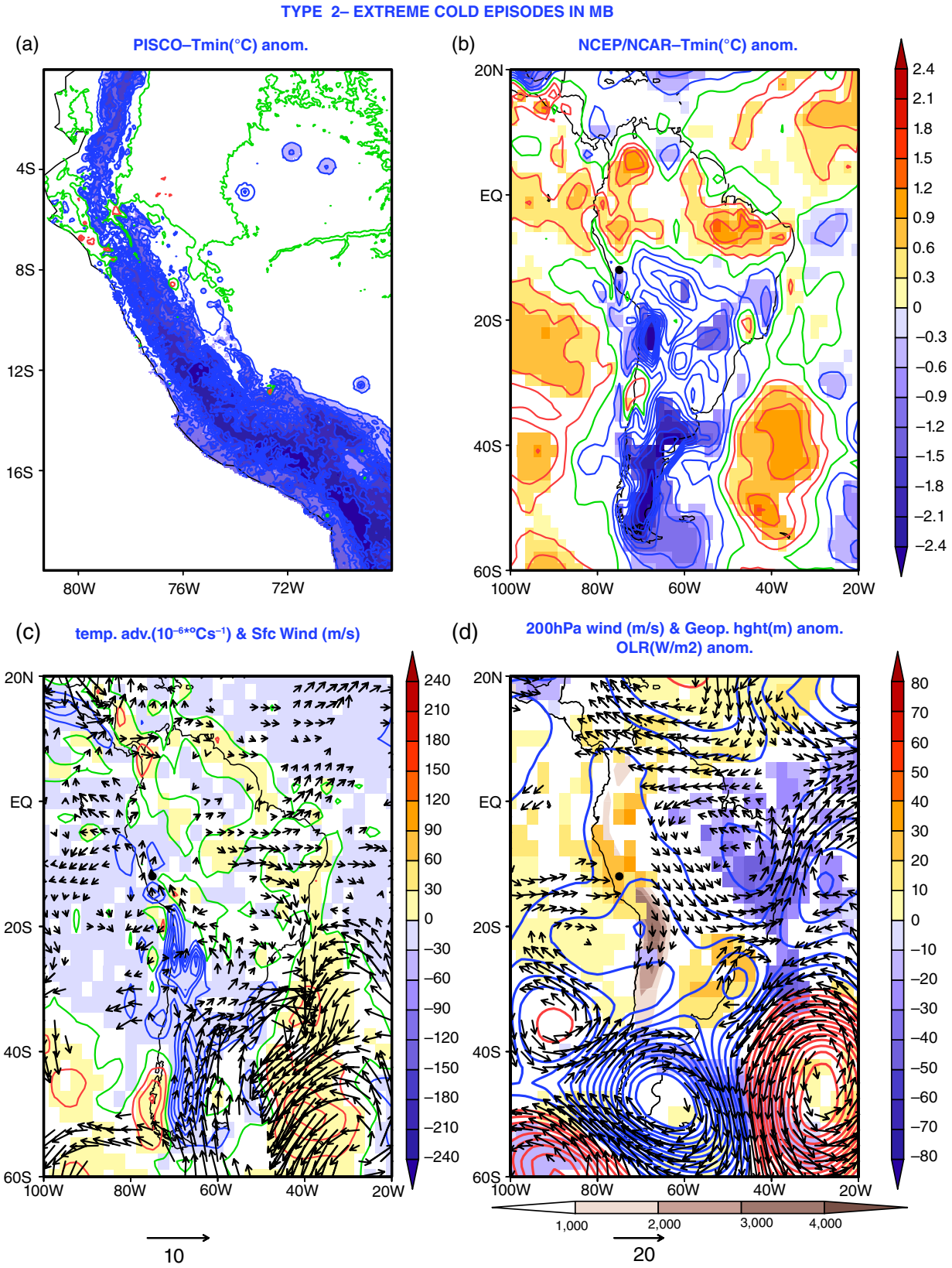

FIGURE 7 As in Figure 6, but for Type-2 extreme cold episodes in the MB during the austral summer [Colour figure can be viewed at wileyonlinelibrary.com]

and +5). Positive OLR anomalies are observed over the MB on day −5, while an OLR dipole is located over the central-northern coast of eastern Brazil (Figure 8a). This OLR dipole is associated with cyclonic circulation over southeastern Brazil (28°S, 46°W) and anticyclonic circulation over northeastern Brazil (15°S, 44°W). The positive OLR anomalies strengthens their intensity over all of Peru, while the intensity of the negative OLR anomalies over NEB weakens on day 0 (Figure 8c). This pattern is consistent with the presence of westerly wind anomalies over Peru, associated

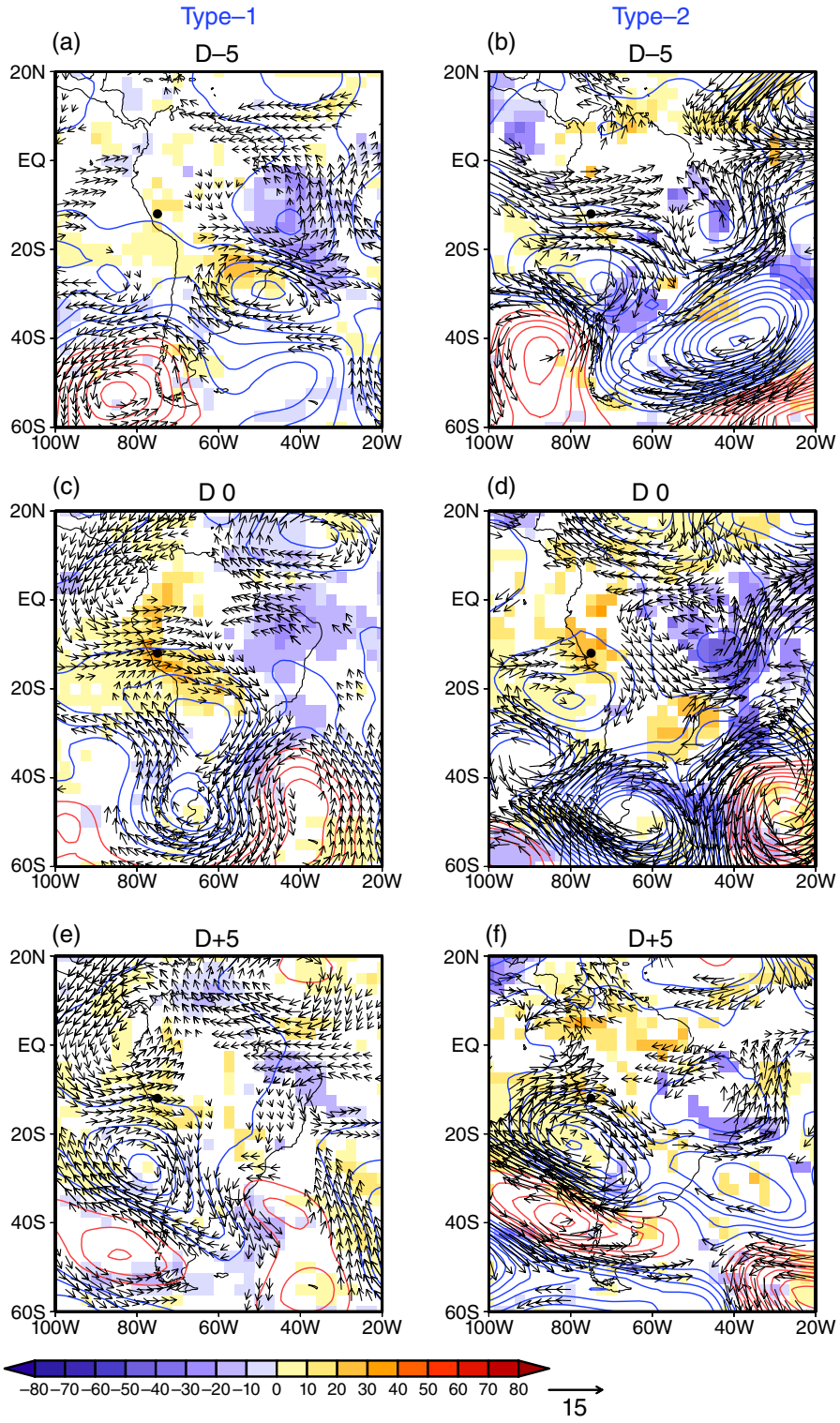

FIGURE 8 Superposed epoch analysis of anomalous fields of OLR (W/m^2) and 200 hPa wind (m/s) and geopotential height (blue (red) contours for negative (positive) anomalies, contour interval is 10 gpm, 0-contour omitted) for (a, c, e) Type-1 and (b, d, f) Type-2 extreme cold episodes in the Mantaro Basin. Analysis based on data during austral summer (JFM) from 1979 to 2010. Black dot indicates location of Mantaro Basin. Analysis based on NCEP-NCAR reanalysis for the 1979–2010 period [Colour figure can be viewed at wileyonlinelibrary.com]

with an anomalous cyclonic circulation over the northern Argentinean Andes (25°S, 65°W), while southeasterly wind anomalies are observed over the northernmost part of NEB. These results indicate a weakening of the Bolivian High during Type-1 ECEs in the MB. The weakening of the BH also is observed on day +5 (Figure 8e), but the OLR dipole between the MB and NEB is weaker with respect to day 0. This circulation is consistent with the presence of westerly wind anomalies, which are linked to the anomalous anticyclonic circulation located off the coast of Colombia (3°N, 78°W) and a cyclonic circulation located over the Peruvian Andes at upper-tropospheric levels. These atmospheric

circulation anomalies suggest that the MJO favours the northward propagation of cold and dry air along the Andes from the southernmost part of the continent toward the Northern Hemisphere during Type-1 ECEs in the MB.

With respect to Type-2 episodes, Figure 8b,d,f show that 200 hPa westerly wind anomalies similarly prevail over the central Peruvian Andes, while southerly wind anomalies are observed over NEB. These results are consistent with a cyclonic circulation located over the northern Chilean Andes (22°S, 82°W) and an anticyclonic circulation located over NEB (2°S, 54°W). This anomalous circulation is again consistent with a weakening of the BH-NL system over SA at upper levels on day −5. Figure 8d,f show that this weakening persists through day 0 and even on to day +5.

5.3 | RMM phases associated with different types of extreme cold episodes in the MB

The results of a composite analysis of OLR and 200 hPa geopotential height anomalies to analyse the role of the RMM Phases 1, 2, 7 and 8 in Type-1 and -2 ECEs in the Mantaro Basin are shown in Figure 9. Figure 9a,e,g show that entire western South America, including the central Peruvian Andes, are under the influence of negative geopotential height anomalies during Type-1 ECEs located on RMM Phases 1, 7 and 8. The same negative OLR anomalies along western SA, which include the central Peruvian Andes, also are observed in Type-2 ECEs that are located on RMM Phases 1, 2 and 8 (Figure 9b,d,h). Although the northward propagation of negative geopotential height anomalies can also be observed in Type-1 ECEs located on RMM Phase 2, they do not propagate northward of 12°S due to the predominance of positive geopotential height anomalies along the equatorial Pacific and tropical South America (Figure 9b). The same feature is observed in Type-2 ECEs located on RMM Phase 7, but the negative OLR anomalies cannot propagate northward of 18°S due to the presence of positive geopotential height anomalies along the equatorial Pacific and tropical SA. These circulation anomalies suggest that Type-1 and Type-2 ECEs in the MB are dynamically linked with RMM Phases 1, 2, 7 and 8 through the northward propagation of cold air advection along the eastern slope of the Andes from southernmost South America toward the Northern Hemisphere.

An additional composite analysis of SST and 200 hPa quasi-geostrophic (QG) stream-function and wave-activity flux anomalies was made to identify the source of the extratropical Rossby wave trains observed during Type-1 and -2 ECEs in the Mantaro Basin located on RMM Phases 1, 2, 7 and 8 (Figures 10 and 11). During Type-1 ECEs, Figure 10a,d show that Type-1 events located on RMM Phases 1 and 8 are linked to positive SST anomalies over southeastern Africa while at the same time upper-level QG stream-function wave trains and northwesterly wave-activity flux anomalies between 30°S and 60°S emanate from southeastern Africa toward South America. These circulation anomalies are consistent with dry conditions over subtropical SA induced by convective activity off the coast of southeastern Africa through extratropical Rossby-wave trains (Hoskins and Ambrizzi, 1993; Drumond and Ambrizzi, 2008). Figure 10b,c show that Type-1 ECEs located on RMM Phases 2 and 7 are linked to a QG stream-function wave train at 200 hPa, and a westerly wave-activity flux that emanates from the subtropical southern Pacific (20–50°S, 130–150°W) toward South America. These results are consistent with an oblique band of positive SST anomalies (35°S, 160°W and 55°S, 115°W) and positive SST anomalies inside the region (35–60°S, 120–150°W) during Type-1 ECEs located on RMM Phase 2 and RMM Phase 7 (Figure 10b,c, respectively). These results further suggest that the oblique band of positive SST anomalies over the subtropical southern Pacific Ocean is associated with the formation of an extratropical Rossby wave train toward SA during RMM Phase 2, while positive SST anomalies over the entire subtropical South Pacific strengthen the circumpolar Rossby wave trains during their propagation toward SA during RMM Phases 7 and 8.

Conversely, Figure 11a–d shows that Type-2 ECEs located on RMM Phases 1–2 and 7–8 are associated with 200 hPa QG stream-function waves and westerly wave-activity flux anomalies, which propagate longitudinally between 35°S and 65°S. Figure 11a–d also shows weak positive SST anomalies over southeastern Africa and the subtropical South Pacific during Type-2 events located on RMM Phases 1, 2, 7 and 8. These results suggest that these positive SST anomalies might be induced during the eastward propagation of the circumpolar Rossby wave train. Hence, Type-2 ECEs located on RMM Phases 1, 2, 7 and 8 are linked dynamically to the eastward propagation of circumpolar Rossby waves that cross SA and propagate northward along the eastern slope of the Andes.

The exact wave number of the 200 hPa extratropical Rossby-wave trains released by the convective activity off southeastern Africa is beyond the scope of this study, but as pointed out by Hoskins and Karoly (1981), it likely involves the identification of the main zonal wave number of the southern planetary wave through one-dimensional FFT (Fast Fourier Transformation) (see also Liu *et al.,* 2005).

6 | INFLUENCE OF THE MJO AND ENSO ON MINIMUM SURFACE TEMPERATURE OVER THE PERUVIAN ANDES DURING AUSTRAL SUMMER

On interannual time-scales, not considering the effects of varying MJO phases, there is no relationship between the frequency of extreme cold episodes in the MB and ENSO. There is no correlation between number of cold episodes during the austral summer and the state of ENSO as measured by the Niño 3.4 index ($r = 0.01$, not shown). One would assume that El Niño might favour the occurrence of extreme cold episodes in the MB by enhancing meridional

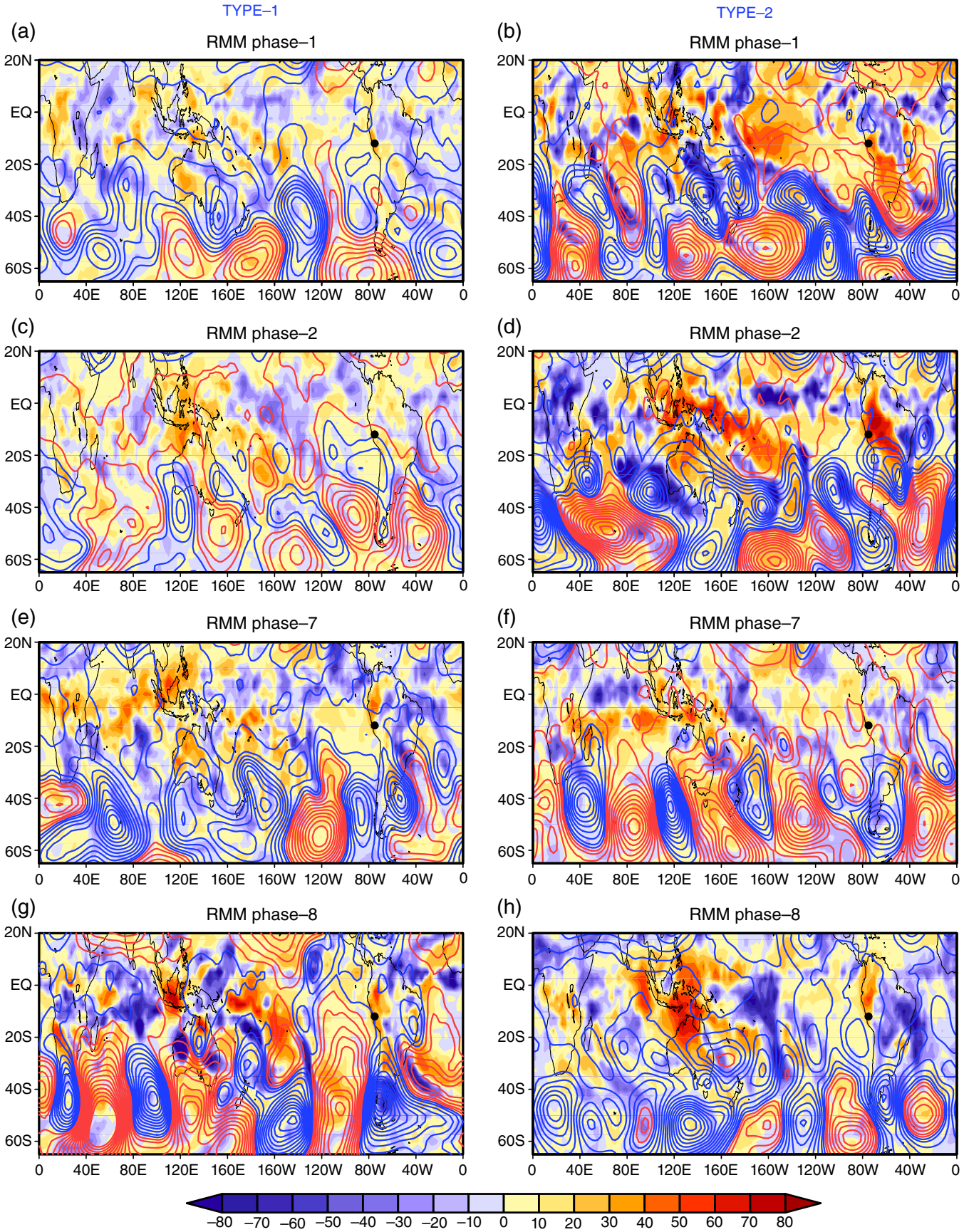

FIGURE 9 Composite anomalies of OLR (W/m^2, shading) and 200 hPa geopotential height (blue (red) contours for negative (positive) anomalies, contour interval is 10 gpm, 0-contour omitted) during (a, c, e, g) Type-1 and (b, d, f, h) Type-2 extreme cold episodes in MB for RMM Phase 1, 2, 7 and 8. Black dot indicates location of Mantaro Basin [Colour figure can be viewed at wileyonlinelibrary.com]

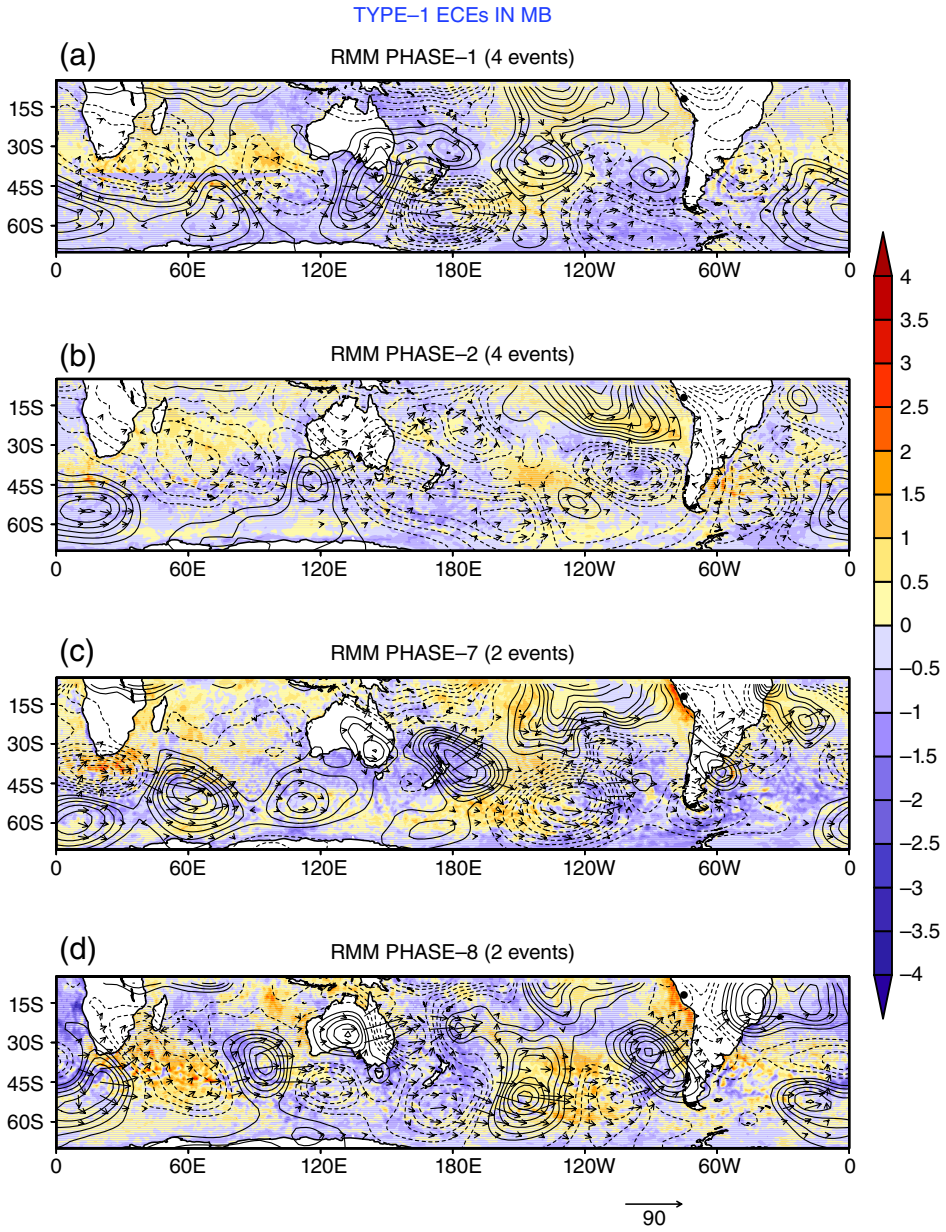

FIGURE 10 Composite anomalies of SST (°C, shading) and 200 hPa quasi-geostrophic stream function (dashed (solid) contours for negative (positive) anomalies, contour interval is 3×10^6 m^2/s, 0-contour omitted) and 200 hPa wave-activity flux (m^2/s^2) anomalies during Type-1 extreme cold episodes in the MB located on RMM Phases 1, 2, 7 and 8 (a, b, c, d). Only wave-activity flux anomalies higher than 8 m^2/s^2 are shown. Black dot indicates location of Mantaro Basin [Colour figure can be viewed at wileyonlinelibrary.com]

baroclinicity over the eastern Pacific, thereby strengthening the upper-level westerly flow over the Peruvian Andes, which in turn inhibits easterly moisture influx and reduces cloud cover over the central Peruvian Andes (Garreaud *et al.,* 2003; Sulca *et al.,* 2018). On the other hand, however, El Niño events tend to warm the circumtropical troposphere, thereby reducing the likelihood of extreme cold events. Given that the correlation is virtually zero, the two competing processes appear to cancel one another.

A composite analysis of JFM *T*min anomalies over Peru during each MJO Phase associated with Neutral years was performed to assess the impact of each Phase on JFM *T*min anomalies over the Peruvian Andes (Figure 12). Figure 12a,b,g,h show negative *T*min anomalies over the central Peruvian Andes from RMM Phase 7 to 2, but they are weakest and strongest in RMM Phase 7 and RMM Phase 1, respectively. Figure 12g,h also show that the negative *T*min anomalies in RMM Phases 7 and 8 are confined to the Mantaro basin while RMM Phases 1 and 2 register negative *T*min anomalies over all of the Peruvian Andes. Nonetheless, the *T*min anomalies seen in the PISCO dataset during RMM Phases 7, 8, 1 and 2 are weaker than the intensity of the extreme cold events in the MB. Conversely, Figure 12c–f shows that positive *T*min anomalies are present over the central Peruvian Andes from RMM Phase 3 to 6, but the weakest and strongest anomalies are observed in Phases 3 and 4, respectively. Figure 12d–f displays that RMM Phases 4, 5 and 6 register positive *T*min anomalies along the tropical

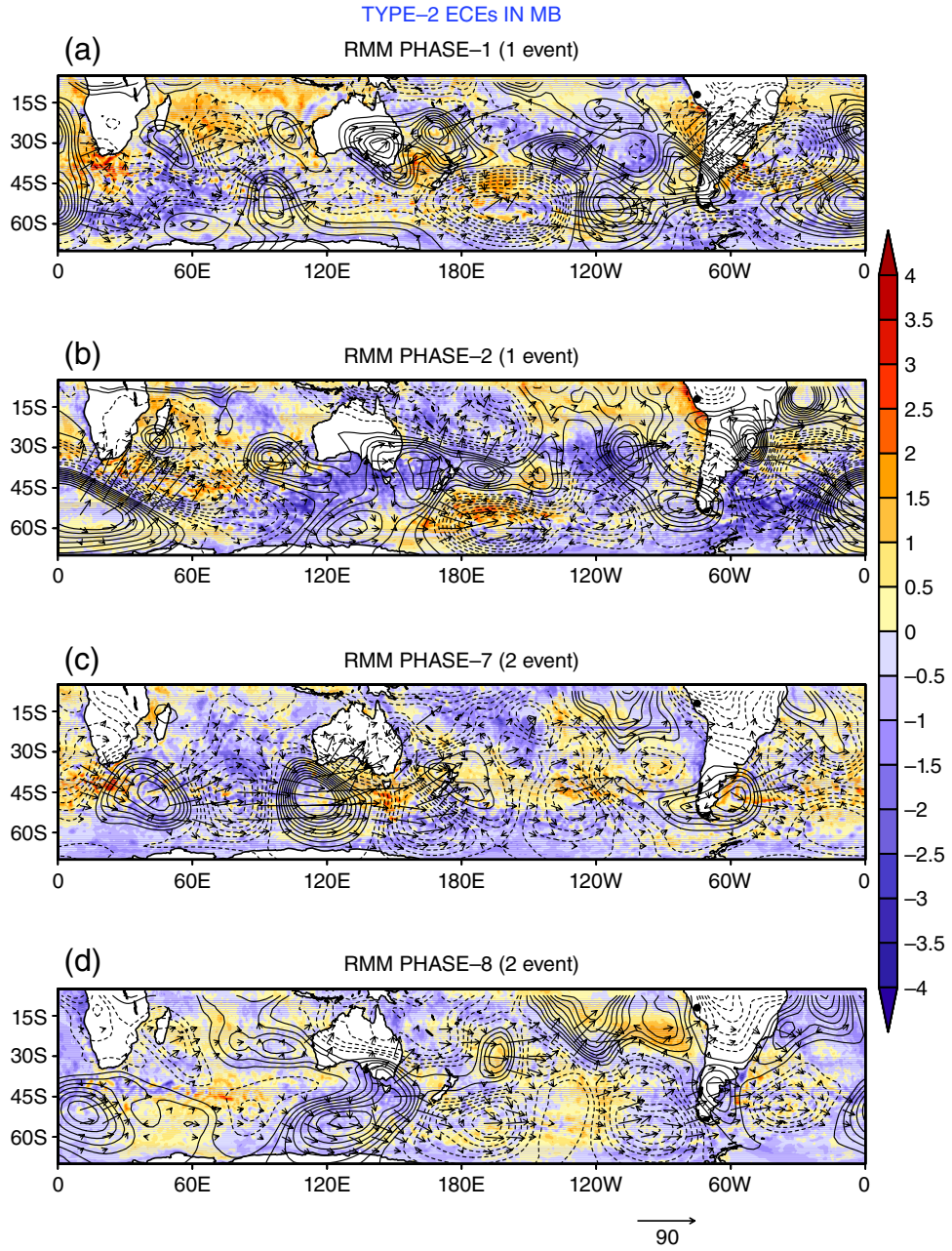

FIGURE 11 (a–d) As in Figure 10, but for Type-2 extreme cold episodes in the MB that only coincide with RMM Phases 7, 8, 1 and 2 [Colour figure can be viewed at wileyonlinelibrary.com]

Andes from northern Chile to Ecuador, while positive *T*min anomalies are confined to the Mantaro basin in RMM Phase 3. These results show that the sign of the *T*min anomalies over the central Peruvian Andes in the RMM Phase 3 and 7 are opposite with respect to those documented in Alvarez *et al.* (2016). This contradiction is likely caused by the higher station density of the PISCO dataset.

In addition, a composite analysis of *T*min anomalies during each MJO phase was performed for El Niño and La Niña events (Figures 13 and 14). During El Niño, Figure 13a,g,h show negative *T*min anomalies over the tropical Andes from northern Chile to Ecuador, but the coldest *T*min values are observed in RMM Phases 7, 8 and 1. El Niño enhances meridional baroclinicity that induces upper-level westerly flow over equatorial and subtropical SA, strengthening the eastward propagation of the MJO during RMM Phases 7, 8 and 1 (Garreaud *et al.,* 2003; Moon *et al.,* 2011; Sulca *et al.,* 2018). The enhanced meridional baroclinicity also strengthens the large-scale subsidence over the central Peruvian Andes during RMM Phase 1 (Moon *et al.,* 2011; Shimizu and Ambrizzi, 2016). Conversely, Figure 13c–f illustrate that positive *T*min anomalies are present over the central Peruvian Andes from RMM Phases 3 to 6, but they only cover all of Peru during RMM Phases 5 and 6. These results are consistent with the effect of a warming circumtropical troposphere during El Niño.

With respect to La Niña, Figure 14h,a,b,c show negative *T*min anomalies over the central Peruvian Andes in RMM Phases 8, 1, 2 and 3; but they are weaker than in Neutral and El Niño years. These results are consistent with the

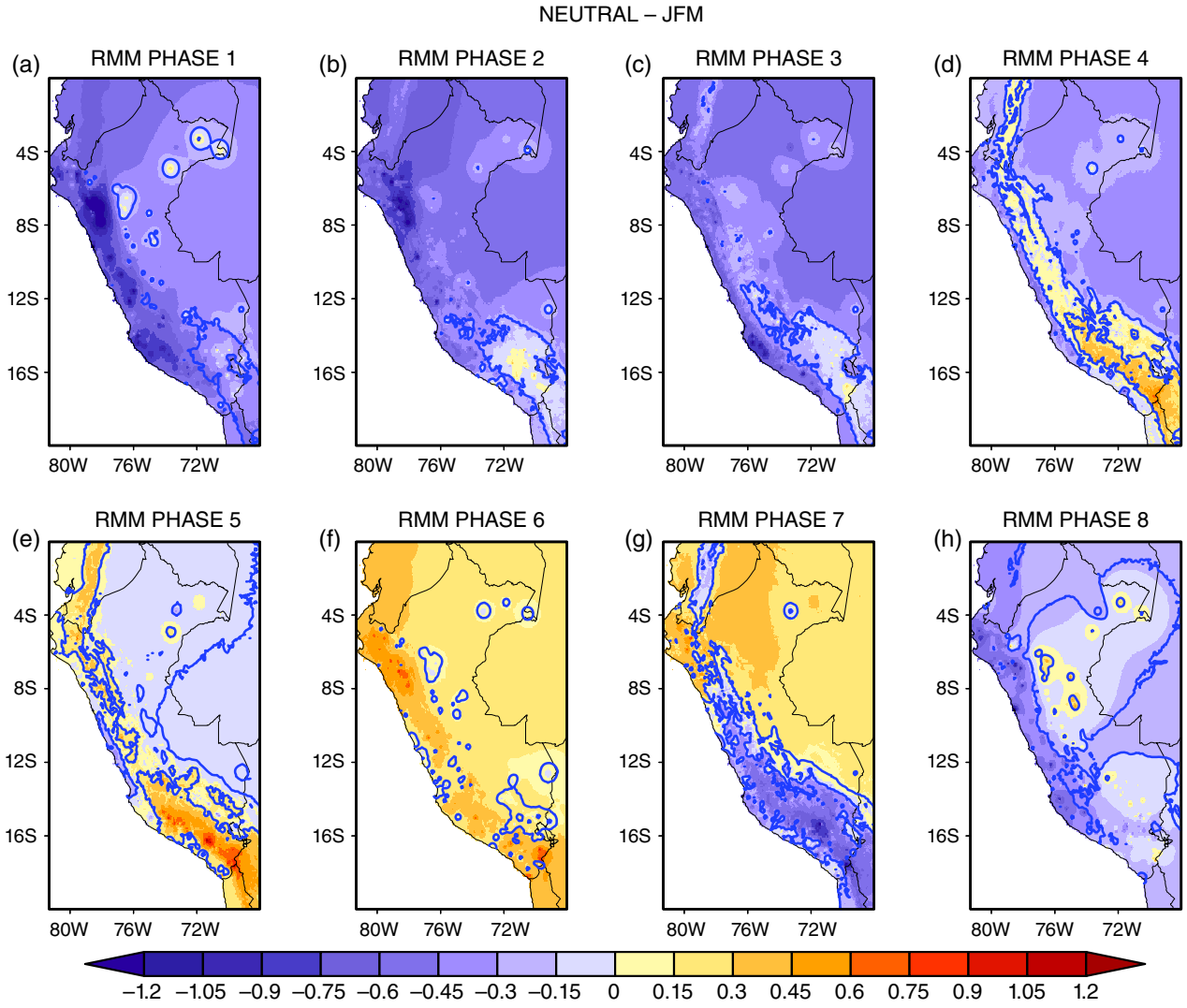

FIGURE 12 (a–h) Composites of JFM minimum surface temperature anomalies for each RMM Phase of MJO during ENSO Neutral years. Blue contours indicate minimum temperature anomalies that are significant at the 90% confidence interval. Contour interval is 0.5 °C and 0-contour is omitted. PISCO dataset was used in this study for the 1981–2010 period [Colour figure can be viewed at wileyonlinelibrary.com]

effect of reduced meridional baroclinicity, which enhances upper-level easterly flow over Peru during La Niña (Garreaud *et al.,* 2003; Moon *et al.,* 2011; Sulca *et al.,* 2018). This upper-level easterly flow favours the influx of moisture from the Amazon basin to the central Peruvian Andes, thereby enhancing deep convection and cloud cover (Garreaud *et al.,* 2003), which tends to reduce night-time and early morning radiative cooling. Conversely, RMM Phases 4, 5, 6 and 7 present positive *T*min anomalies over the central Peruvian Andes (Figure 14d–g). The positive *T*min anomalies are restricted to the central-southern Peruvian Andes during RMM Phases 4 and 7 (Figure 14d,g) while RMM Phases 5 and 7 feature positive *T*min anomalies over all the tropical Andes from northern Chile to Ecuador (Figure 14e,f).

7 | SUMMARY AND CONCLUSIONS

Extreme cold episodes in the Mantaro basin have a duration of only 1–2 days and are characterized by a sharp drop in minimum temperature of, on average, approximately 1.97 ± 0.86°C between day −1 and day 0. The short-lived nature of these events is apparent when considering that 91.08% of all extreme cold episodes have an average duration of 2 days or less, while extreme cold events with long duration (more than 5 days) only occur 1.78% of the time.

Extreme cold episodes in the Mantaro basin appear to be caused by cold air advection associated with equatorward propagation of midlatitude Rossby wave trains to the east of the Andes at night-time or early morning. The equatorward propagation of cold and dry air masses reduces cloud cover and inhibits moisture influx, convective activity and hence cloud formation. Furthermore, the cold advection weakens the Bolivian High–Nordeste Low (BH-NL) system over SA at upper-tropospheric levels. The observed teleconnection between the Bolivian High and the Nordeste Low explains the observed *T*min dipole pattern with NEB during extreme cold episodes in the MB. Furthermore, this *T*min dipole is consistent with an observed OLR dipole of opposite sign between the MB and NEB.

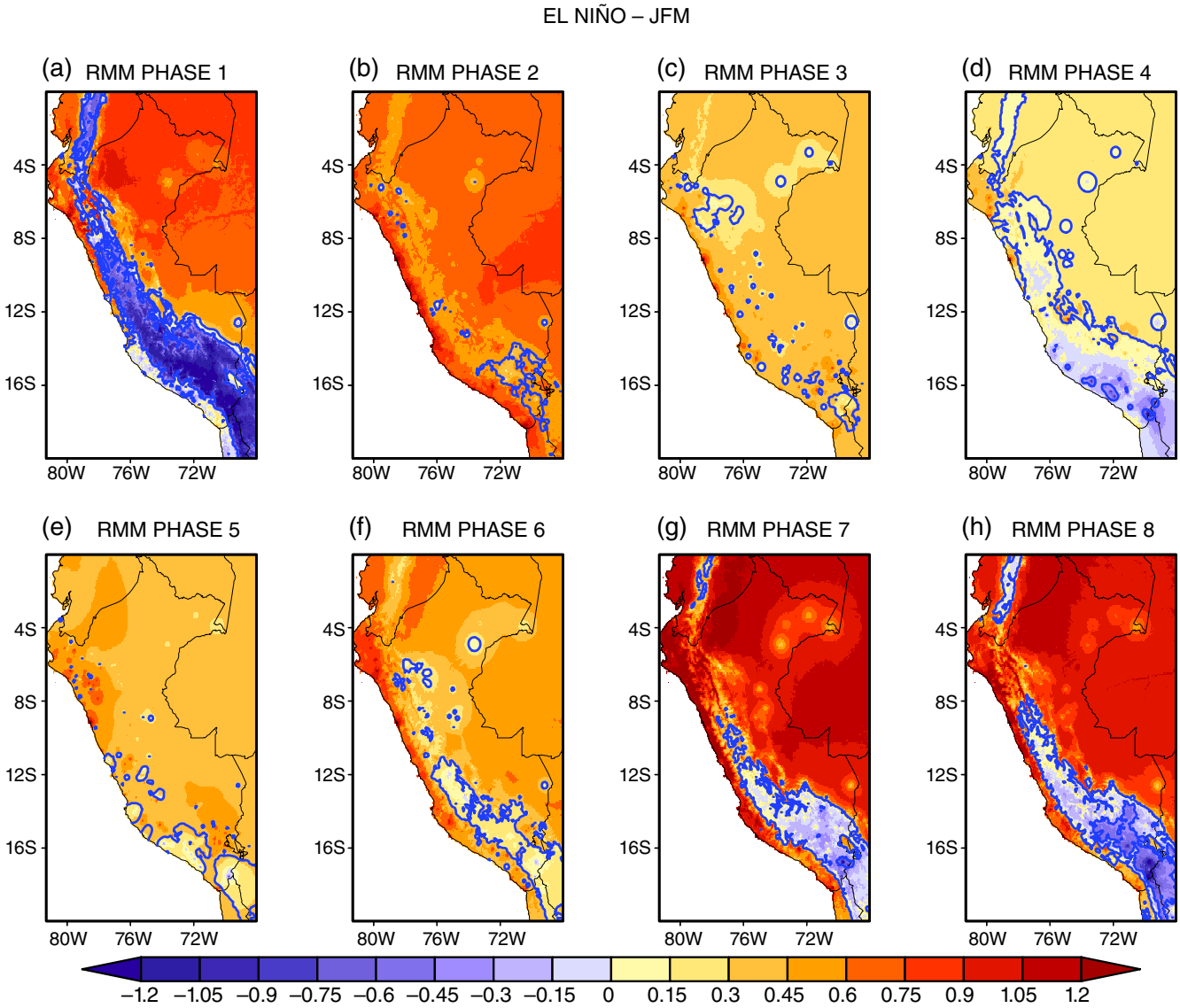

FIGURE 13 (a–h) As in Figure 12, but for El Niño years [Colour figure can be viewed at wileyonlinelibrary.com]

On intraseasonal time-scales, the Madden–Julian Oscillation favours the northward propagation of cold and dry air, along the eastern slope of the Andes and thus leads to Type-1 and -2 ECEs in the MB. Type-1 events are associated with a weakening of the Bolivian High at upper-tropospheric levels. Furthermore, Type-1 events are related to suppressed periods of the MJO, favouring the northward propagation of cold and dry air along the Andes. Type-1 ECEs located on RMM Phases 1 and 8 are linked dynamically with extratropical Rossby wave trains emanating from southeastern Africa (i.e. warm SST conditions) while Type-1 events located on RMM Phases 2 and 7 are associated with circumpolar Rossby wave trains that are strengthened when they cross the subtropical South Pacific (i.e. warm SST anomalies). Conversely, Type-2 events are associated with a weakening of the entire Bolivian High–Nordeste Low (BH-NL) system over SA at upper-tropospheric levels. Furthermore, Type-2 events are related to periods of enhanced convective activity of the MJO, favouring the northward propagation of cold and dry air along the Andes. Furthermore, Type-2 events located on RMM Phases 1–2 and 7–8 are associated with circumpolar Rossby wave trains.

The MJO is associated with ECEs in the Mantaro basin during austral summer. Fifty-nine per cent of all Type-1 ECEs in the MB are associated with RMM Phases 7, 8, 1 and 2; they feature a weakened Bolivian High induced by the northward propagation of cold and dry air along the Andes. Eighty-six per cent of all Type-2 ECEs in the MB coincide with MJO Phases 7, 8, 1 and 2. They occur in association with a weakened Bolivian High–Nordeste Low system and also feature a northward propagation of cold and dry air along the Andes.

On interannual time-scales, no clear pattern or forcing emerged. The El Niño–Southern Oscillation phenomenon is not significantly correlated with extreme cold episode occurrence. ENSO does, however, modulate the impact of the MJO on minimum temperature over the central Peruvian Andes during austral summer. Both ENSO phases (i.e. El Niño and La Niña) strengthen negative minimum temperature anomalies over the Mantaro basin during MJO Phases 7–8

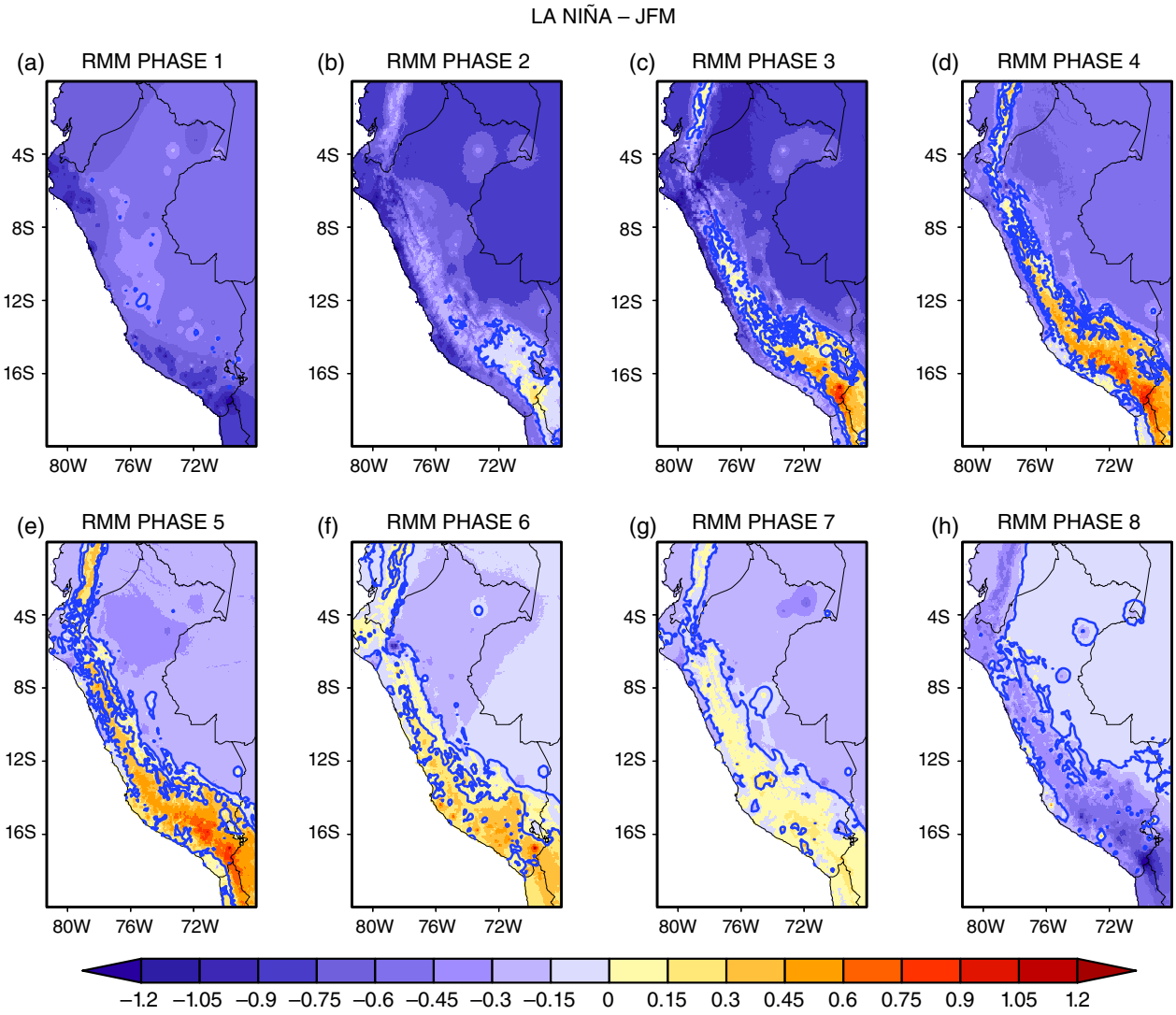

FIGURE 14 (a–h) As in Figure 12, but for La Niña years [Colour figure can be viewed at wileyonlinelibrary.com]

while they weaken positive minimum temperature anomalies over the MB during MJO Phases 3–6. El Niño also induces positive minimum temperature anomalies over all of the Peruvian Andes during MJO Phase 2.

ACKNOWLEDGEMENTS

The authors are grateful for funding obtained from the US State Department (award S-LMAQM-11-GR-086 under the ACCION umbrella to M. Vuille), and would like to thank the National Peruvian Weather Service (SENAMHI) and the Instituto Geofísico del Perú (IGP) for providing daily minimum temperature data from climatological stations in the Mantaro basin, W. Lavado-Casimiro and A. Huerta for providing gridded daily minimum temperature from the PISCO dataset and N. Quispe for useful comments in the initial part of this study. We are very grateful to two anonymous reviewers who provided us with valuable comments, which helped us to significantly advance our results and to substantially improve the article. This work was performed using computational resources, HPC-Linux-Cluster, from the Laboratorio de Dinámica de Fluidos Geofísicos Computacionales (http://scah.igp.gob.pe/laboratorios/dfgc) at the Instituto Geofísico del Perú (grants 101-2014-FONDECYT, SPIRALES2012 IRD-IGP, Manglares IGP-IDRC#106714, PPR 068 programme).

ORCID

Juan Sulca https://orcid.org/0000-0003-4393-3161
Mathias Vuille https://orcid.org/0000-0002-9736-4518
Ken Takahashi https://orcid.org/0000-0003-3670-2939
Jhan-Carlo Espinoza https://orcid.org/0000-0001-7732-8504
Yamina Silva https://orcid.org/0000-0003-0653-0224
Grace Trasmonte https://orcid.org/0000-0003-4927-0493
Ricardo Zubieta https://orcid.org/0000-0002-4315-7695

REFERENCES

Alvarez, M.S., Vera, C.S., Kiladis, G.N. and Liebmann, B. (2016) Influence of the Madden–Julian oscillation on precipitation and surface air temperature in South America. *Climate Dynamics*, 46(1), 245–262. https://doi.org/10.1007/s00382-015-2581-6.

Ambrizzi, T. and Hoskins, B.J. (1997) Stationary Rossby-wave propagation in a baroclinic atmosphere. *Quarterly Journal of the Royal Meteorological Society*, 123, 919–928. https://doi.org/10.1002/qj.49712354007.

Berbery EH, Nogües-Paegle J, Horel JD. (1992) Wavelike Southern Hemisphere extratropical teleconnections. *Journal of the Atmospheric Sciences*, 49(2):, 155–177. https://doi.org/10.1175/1520-0469(1992)049<2347:C>2.0.CO;2.

Carvalho LMV, Jones C, Liebmann B. (2004) The South Atlantic convergence zone: persistence, intensity, form, extreme precipitation and relationships with intraseasonal activity. *Journal of Climate*, 17, 88–108. https://doi.org/10.1175/1520-0442(2004)017<0088:TSACZI>2.0.CO;2.

Chen T, Weng S, Schubert S. (1999) Maintenance of austral summer-time upper tropospheric circulation over tropical South America: the Bolivian high–Nordeste low system. *Journal of the Atmospheric Sciences*, 56, 2081–2100. https://doi.org/10.1175/1520-0469(1999)056<2081:MOASUT>2.0.CO;2.

Dirección Regional de Agricultura – JUNÍN. (2010) *Intensiones de siembra para la campaña agrícola del 2010*. Junín: Ministerio de Agricultura.

Drumond, A.R. and Ambrizzi, T. (2008) The role of the South Indian and Pacific Oceans in South America monsoon system. *Theoretical and Applied Climatology*, 94, 125–137. https://doi.org/10.1007/s00704-007-0358-5.

Espinoza, J.C., Lengaigne, M., Ronchail, J. and Janicot, S. (2012) Large-scale circulation patterns and related rainfall in the Amazon basin: a neuronal networks approach. *Climate Dynamics*, 38(1–2), 121–140. https://doi.org/10.1007/s00382-011-1010-8.

Espinoza, J.C., Ronchail, J., Lengaigne, M., Quispe, N., Silva, Y., Bettolli, M.L., Avalos, G. and Llacza, A. (2013) Revisiting wintertime cold air intrusions at the east of the Andes: propagating features from subtropical Argentina to Peruvian Amazon and relationship with large-scale circulation patterns. *Climate Dynamics*, 41(7–8), 1983–2002. https://doi.org/10.1007/s00382-012-1639-y.

Figueroa S, Satyamurty P, Da Silva P. (1995) Simulations of the summer circulation over the South American region with an Eta coordinate model. *Journal of the Atmospheric Sciences*, 52, 1573–1584. https://doi.org/10.1175/1520-0469(1995)052<1573:SOTSCO>2.0.CO;2.

Fuenzalida, H.A., Sanchez, R. and Garreaud, R.D. (2005) A climatology of cutoff lows in the Southern Hemisphere. *Journal of Geophysical Research*, 110, D18101. https://doi.org/10.1029/2005JD005934.

Garreaud R. (1999a) Multiscale analysis of the summertime precipitation over the central Andes. *Monthly Weather Review*, 127, 901–921. https://doi.org/10.1175/1520-0493(1999)127<0901:MAOTSP>2.0.CO;2.

Garreaud R. (1999b) Cold air incursions over subtropical and tropical South America: a numerical case study. *Monthly Weather Review*, 127, 2823–2853. https://doi.org/10.1175/1520-0493(1999)127<2823:CAIOSA>2.0.CO;2.

Garreaud R, Vuille M, Clement A. (2003) The climate of the Altiplano: observed current conditions and mechanisms of past changes. *Palaeogeography, Palaeoclimatology, Palaeoecology*, 194, 5–22. https://doi.org/10.1016/S0031-0182(03)00269-4.

Garreaud, R., Vuille, M., Compagnucci, R. and Marengo, L. (2009) Present-day South American climate. *Palaeogeography, Palaeoclimatology, Palaeoecology*, 281, 180–195. https://doi.org/10.1016/j.palaeo.2007.10.032.

Garreaud RD. (2000) Cold air incursions over subtropical South America: mean structure and dynamics. *Monthly Weather Review*, 128, 2544–2559. https://doi.org/10.1175/1520-0493(2000)128<2544:CAIOSS>2.0.CO;2.

Garreaud RD, Aceituno P. (2001) Interannual rainfall variability over the South American Altiplano. *Journal of Climate*, 14, 2779–2789. https://doi.org/10.1175/1520-0442(2001)014<2779:IRVOTS>2.0.CO;2.

Garreaud, R.D. and Fuenzalida, H.A. (2007) The influence of the Andes on cutoff lows: a modelling study. *Monthly Weather Review*, 135, 1596–1613. https://doi.org/10.1175/MWR3350.1.

Garreaud RD, Wallace JM. (1997) The diurnal march of convective cloudiness over the Americas. *Monthly Weather Review*, 125, 3157–3171. https://doi.org/10.1175/1520-0493(1997)125<3157:TDMOCC>2.0.CO;2.

Gill, A.E. (1980) Some simple solutions for heat-induced tropical circulation. *Quarterly Journal of the Royal Meteorological Society*, 106, 447–462. https://doi.org/10.1002/qj.49710644905.

Giraldez, L. and Trasmonte, G. (2012) Impactos de heladas en la agricultura del valle del Mantaro. In: Martínez, A.G (Ed.), *Libro Manejo de riesgos de desastres ante eventos meteorológicos extremos en el valle del Mantaro. Volumen II. Resultados del proyecto MAREMEX*. Lima: Instituto Geofísico del Perú.

Gruber, A. and Krueger, A.F. (1984) The status of the NOAA outgoing longwave radiation data set. *Bulletin of the American Meteorological Society*, 65(9), 958–962. https://doi.org/10.1175/1520-0477(1984)065<0958:TSOTNO>2.0.CO;2.

Hoskins BJ, Ambrizzi T. (1993) Rossby wave propagation on a realistic longitudinally varying flow. *Journal of the Atmospheric Sciences*, 50(12), 1661–1671. https://doi.org/10.1175/1520-0469(1993)050<1661:RWPOAR>2.0.CO;2.

Hoskins, B.J. and Karoly, D.J. (1981) The steady linear response of a spherical atmosphere to thermal and orographic forcing. *Journal of the Atmospheric Sciences*, 38, 1179–1196.

Huerta, A., Lavado-Casimiro, W., Aybar, C. and Sabino, E. (2017) *Desarrollo de datos grillados de temperatura diaria en Perú*. Lima: Servicio Nacional de Meteorología e Hidrología del Perú.

Hurley, J.V., Vuille, M., Hardy, D.R., Burns, S. and Thompson, L.G. (2015) Cold air incursions, $\delta^{18}O$ variability and monsoon dynamics associated with snow days at Quelccaya Ice Cap. *Peru. Journal of Geophysical Research*, 120, 7467–7487. https://doi.org/10.1002/2015JD023323.

Instituto Geofísico del Perú. (2005) *Atlas Climatológico de precipitaciones y temperaturas en la Cuenca del Mantaro*. Lima: Fondo Editorial CONAM.

Junquas, C., Li, L., Vera, C.S., Le Treut, H. and Takahashi, K. (2016) Influence of South America orography on summertime precipitation in southeastern South America. *Climate Dynamics*, 46(11–12), 3941–3963. https://doi.org/10.1007/s00382-016-3061-3.

Kalnay E, Kanamitsu M, Kistler R, Collins W, Deaven D, Gandin L, Iredell M, Saha S, White G, Woollen J, Zhu Y, Leetmaa A, Reynolds R, Chelliah M, Ebisuzaki W, Higgins W, Janowiak J, Mo KC, Ropelewski C, Wang J, Jenne R, Joseph D. (1996) The NCEP/NCAR 40-years reanalysis project. *Bulletin of the American Meteorological Society*, 77, 437–472. https://doi.org/10.1175/1520-0477(1996)077<0437:TNYRP>2.0.CO;2.

Kessler, W.S. (2001) EOF representations of the Madden–Julian Oscillation and its connection with ENSO. *Journal of Climate*, 14, 3055–3061. https://doi.org/10.1175/1520-0442(2001)014<3055:EROTMJ>2.0.CO;2.

Kodama, Y. (1992) Large-scale common features of subtropical precipitation zones (the Baiu frontal zone, the SPCZ and the SACZ). Part I: Characteristics of subtropical frontal zones. *Journal of the Meteorological Society of Japan*, 70(4), 813–836. https://doi.org/10.2151/jmsj1965.70.4_813.

Kousky, V.E. (1979) Frontal influences on northeast Brazil. *Monthly Weather Review*, 107, 1140–1153. https://doi.org/10.1175/1520-0493(1979)107,1140:FIONB.2.0.CO;2.

Kousky, V.E. and Gan, M.A. (1981) Upper tropospheric cyclonic vortices in the tropical South Atlantic. *Tellus*, 33A, 538–551. https://doi.org/10.1111/j.2153-3490.1981.tb01780.x.

Lenters JD, Cook KH. (1997) On the origin of the Bolivian high and related circulation features of the South American climate. *Journal of the Atmospheric Sciences*, 54, 656–677. https://doi.org/10.1175/1520-0469(1997)054<0656:OTOOTB>2.0.CO;2.

Liebmann B, Kiladis GN, Marengo JA, Ambrizzi T, Glick J. (1999) Submonthly convective variability over South America and the South Atlantic Convergence Zone. *Journal of Climate*, 12, 1877–1891. https://doi.org/10.1175/1520-0442(1999)012<1877:SCVOSA>2.0.CO;2.

Liebmann, B. and Smith, C.A. (1996) Description of a complete (interpolated) outgoing longwave radiation dataset. *Bulletin of the American Meteorological Society*, 77, 1275–1277.

Liu, N., Chen, H., Chen, X., Pan, Z. and Tao, Y. (2005) A dynamic view of the tropospheric teleconnection between IOD and the Pacific Ocean. *Chinese Science Bulletin*, 50(19), 2249–2253. https://doi.org/10.1360/982004-739.

Lupo AL, Nocera JJ, Bosart LF, Hoffman EG, Knight DJ. (2001) South American cold surges: types, composites, and case studies. *Monthly Weather Review*, 129, 1021–1041. https://doi.org/10.1175/1520-0493(2001)129<1021:SACSTC>2.0.CO;2.

Madden RA, Julian PR. (1972) Description of global-scale circulation cells in the Tropics with a 40–50 day period. *Journal of the Atmospheric Sciences*, 29, 1109–1123. https://doi.org/10.1175/1520-0469(1972)029<1109:DOGSCC>2.0.CO;2.

Madden RA, Julian PR. (1994) Observations of the 40–50 day tropical oscillation: a review. *Monthly Weather Review*, 122, 814–837. https://doi.org/10.1175/1520-0493(1994)122<0814:OOTDTO>2.0.CO;2.

Marengo, J.A., Liebmann, B., Grimm, A.M., Misra, V., Silva Dias, P.L., Cavalcanti, I.F.A., Carvalho, L.M.V., Berbery, E.H., Ambrizzi, T., Vera, C.S., Saulo, A.C., Nogües-Paegle, J., Zipser, E., Seth, A. and Alves, L.M. (2012) Recent developments on the South American monsoon system. *International Journal of Climatology*, 32, 1–12. https://doi.org/10.1002/joc.2254.

McPhaden, M.J., Zebiak, S.E. and Glantz, S.E. (2006) ENSO as an integrating concept in Earth science. *Science*, 314(5806), 1740–1745.

Metz, N., Archambault, H.M., Srock, A.F., Galarneau, T.J., Jr. and Bosart, L.F. (2013) A comparison of South American and African preferential pathways

for extreme cold events. *Monthly Weather Review*, 141, 2066–2086. https://doi.org/10.1175/MWR-D-12-00202.1.

Montes de Oca, I. (1995) Geography and climate of Bolivia. *Bulletin de l'Institut Français d'Etudes Andines*, 24, 357–368.

Moon, J.-Y., Wang, B. and Ha, K.-J. (2011) ENSO regulation of MJO teleconnection. *Climate Dynamics*, 37, 1133–1149. https://doi.org/10.1007/s00382-010-0902-3.

Paccini, L., Espinoza, J.C., Ronchail, J. and Segura, H. (2018) Intraseasonal rainfall variability in the Amazon basin related to large-scale circulation patterns: a focus on western Amazon–Andes transition region. *International Journal of Climatology*, 38, 2386–2399. doi:10.1002/joc.5341

Plumb RA. (1985) On the three-dimensional propagation of stationary waves. *Journal of the Atmospheric Sciences*, 42, 217–229. https://doi.org/10.1175/1520-0469(1985)042<0217:OTTDPO>2.0.CO;2.

Reboita, M.S., Nieto, R., Gimeno, L., Porfirio da Rocha, R., Ambrizzi, T., Garreaud, R. and Krüger, L.F. (2010) Climatological features of cutoff lows systems in the Southern Hemisphere. *Journal of Geophysical Research*, 115(D17104), 1–15. https://doi.org/10.1029/2009JD013251.

Reynolds, R.W., Smith, T.M., Liu, C., Chelton, D.B., Casey, K.S. and Schlax, M.G. (2007) Daily high-resolution-blended analyses for sea surface temperature. *Journal of Climate*, 20, 5473–5496. https://doi.org/10.1175/2007JCLI1824.1.

Ropelewski CF, Halpert MS. (1987) Global and regional scale precipitation patterns associated with the El Niño/Southern Oscillation. *Monthly Weather Review*, 115, 1606–1626. https://doi.org/10.1175/1520-0493(1987)115<1606:GARSPP>2.0.CO;2.

Roundy, P.E. (2012a) Tracking and prediction of large-scale organized tropical convection by spectrally focused two-step space-time EOF analysis. *Quarterly Journal of the Royal Meteorological Society*, 138, 919–931. https://doi.org/10.1002/qj.962.

Roundy, P.E. (2012b) Tropical–extratropical interactions. In: Lau, W.K.-M. and Waliser, D.E. (Eds.) *Intraseasonal Variability of the Atmosphere–Ocean Climate System*, 2nd edition. Springer-Verlag Berlin Heidelberg: Springer, pp. 497–512.

Saavedra M, Takahashi K. (2017) Physical controls and frost events in the Central Andes of Peru using *in situ* observations and energy flux models. *Agricultural and Forest Meteorology*, 239, 58–70. htpps://doi.org/10.1016/j.agrformer.2017.02.019.

Schubert SD, Park C-K. (1991) Low-frequency intraseasonal tropical–extratropical circulation. *Journal of the Atmospheric Sciences*, 48, 629–650. https://doi.org/10.1175/1520-0469(1991)048<0629:LFITEI>2.0.CO;2.

Shimizu, M.H. and Ambrizzi, T. (2016) MJO influence on ENSO effects in precipitation and temperature over South America. *Theoretical and Applied Climatology*, 124(1–2), 291–301. https://doi.org/10.1007/s00704-015-1421-2.

Sicart, J.E., Espinoza, J.C., Queno, L. and Medina, M. (2016) Radiative properties of clouds over a tropical Bolivian glacier: seasonal variations and relationship with regional atmospheric circulation. *International Journal of Climatology*, 36, 3116–3128. https://doi.org/10.1002/joc.4540.

Smith, T.M., Reynolds, R.W., Peterson, T.C. and Lawrimore, J. (2008) Improvements to NOAAs historical merged land–ocean surface temperature analysis (1880–2006). *Journal of Climate*, 21, 2283–2296. https://doi.org/10.1175/2007JCLI2100.1.

Sulca, J., Takahashi, K., Espinoza, J.C., Vuille, M. and Lavado-Casimiro, W. (2018) Impacts of different ENSO flavors and tropical Pacific convection variability (ITCZ, SPCZ) on austral summer rainfall in South America, with a focus on Peru. *International Journal of Climatology*, 38(1), 420–435. https://doi.org/10.1002/joc.5185.

Sulca, J., Vuille, M., Silva, Y. and Takahashi, K. (2016) Teleconnections between the Peruvian central Andes and northeast Brazil during extreme rainfall events. *Journal of Hydrometeorology*, 17, 499–515. https://doi.org/10.1175/JHM-D-15-0034.1.

Takaya K, Nakamura H. (2001) A formulation of a phase-independent wave-activity flux for stationary and migratory quasigeostrophic eddies on zonally varying basic flow. *Journal of the Atmospheric Sciences*, 58, 608–627. https://doi.org/10.1175/1520-0469(2001)058<0608:AFOAPI>2.0.CO;2.

Trasmonte, G., Chavez, R., Segura, B. and Rosales, J.L. (2008) Frost risks in the Mantaro river basin. *Advances in Geosciences*, 14, 265–270. https://doi.org/10.5194/adgeo-14-265-2008.

Trasmonte, G., Silva, Y., Segura, B. and Latínez, K. (2010) *Variabilidad de las temperaturas máximas y mínimas en el Valle del río Mantaro*. In: Vidal, Y.S. (Ed.), *Memoria del Subproyecto "Pronóstico estacional de lluvias y temperaturas en la cuenca del río Mantaro, para su aplicación den la agricultura 2007–2010"*, Instituto Geofisico del Perú: Lima-Peru, pp. 37–49.

Trenberth, K.E., Branstator, G.W., Karoly, D., Kumar, A., Lau, N. and Ropelewski, C. (1998) Progress during TOGA in understanding and modelling global teleconnections associated with tropical sea surface temperatures. *Journal of Geophysical Research*, 103(C7), 14291–14324.

Vera, C., Higgins, W., Amador, J., Ambrizzi, T., Garreaud, R., Gochis, D., Gutzler, D., Lettenmaier, D., Marengo, J., Mechoso, C.R., Nogües-Paegle, J., Silva Dias, P.L. and Zhang, C. (2006) Towards a unified view of the American monsoon systems. *Journal of Climate*, 15, 1591–1608. https://doi.org/10.1175/JCLI3896.1.

Vera C, Silvestri G, Barros V, Carril A. (2004) Differences in El Niño response over the Southern Hemisphere. *Journal of Climate*, 17(9), 1741–1753. https://doi.org/10.1175/1520-0442(2004)017<1741:DIENRO>2.0.CO;2.

Vuille, M., Bradley, R.S. and Keimig, F. (2000) Interannual climate variability in the Central Andes and its relation to tropical Pacific and Atlantic forcing. *Journal of Geophysical Research*, 105(12), 447–460. https://doi.org/10.1029/2000JD900134.

Vuille M, Keimig F. (2004) Interannual variability of summertime convective cloudiness and precipitation in the central Andes derived from ISCCP-B3 data. *Journal of Climate*, 17, 3334–3348. https://doi.org/10.1175/1520-0442(2004)017<3334:IVOSCC>2.0.CO;2.

Wilks, S.D. (2011) *Statistical methods in the atmospheric sciences*. In: Dmowska, R., Hartmann, D. and Rossby, H.T. (Eds.), *International Geophysics Series*, Vol. 100. San Diego, CA, USA: Academic Press.

Wheeler, M.C. and Hendon, H.H. (2004) An all-season real-time multivariate MJO index: development of an index for monitoring and prediction. *Monthly Weather Review*, 132, 1917–1932. https://doi.org/10.1175/1520-0493(2004)132<1917:AARMMI>2.0.CO;2.

Zubieta, R. (2010) *Procesamiento digital de imágenes de satélite y elaboración del mapa de uso de la tierra del valle del Mantaro*. In: *Libro Memoria del subproyecto "Pronóstico estacional de lluvias y temperaturas en la cuenca del río Mantaro para su aplicación en la agricultura 2007-2010"*. Lima: Instituto Geofísico del Perú.

Zubieta, R., Quijano, J., Latínez, K. and Guillermo, P. (2012) *Evaluación de las zonas de peligro frente a inundaciones por máximas avenidas en el valle del río Mantaro*. In: *Manejo de riesgos de desastres ante eventos meteorológicos extremos en el valle del Mantaro*, Vol. II, Proyecto MAREMEX Mantaro. Lima: Instituto Geofísico del Perú.

Zubieta, R., Saavedra, M., Silva, Y. and Giraldez, L. (2016) Spatial analysis and temporal trends of daily precipitation concentration in the Mantaro River basin – central Andes of Peru. *Stochastic Environmental Research and Risk Assessment*, 31, 1305–1318.

How to cite this article: Sulca J, Vuille M, Roundy P, *et al*. Climatology of extreme cold events in the central Peruvian Andes during austral summer: origin, types and teleconnections. *Q J R Meteorol Soc* 2018;144:2693–2714. https://doi.org/10.1002/qj.3398